Well layout optimization for groundwater heat pump systems using the adjoint approach

Smajil Halilovic[a,*], Fabian Böttcher[b], Stephan C. Kramer[c], Matthew D. Piggott[c], Kai Zosseder[b], Thomas Hamacher[a]

[a] *Technical University of Munich, Chair of Renewable and Sustainable Energy Systems, Germany*
[b] *Technical University of Munich, Chair of Hydrogeology, Germany*
[c] *Imperial College London, Department of Earth Science and Engineering, United Kingdom*

Abstract

Groundwater heat pump systems cause thermal anomalies in the aquifer that can impact upon downstream systems and reduce their efficiency. Therefore, it is important to optimally position the extraction and injection wells of such systems to avoid negative interactions and maximize the thermal potential of the aquifer. This paper presents a new method to determine optimal well layouts of groundwater heat pumps using the adjoint approach, which is an efficient way to solve the underlying PDE-constrained optimization problem. An integral part of the method is the numerical groundwater simulation, which here is based on the finite element method. In addition, a multi-start initialization strategy is introduced in an attempt to better reach the global optimum. The method is applied to a real case study with 10 groundwater heat pumps, i.e. 20 wells, and two optimization scenarios with different natural groundwater temperatures. In both scenarios, the optimization method successfully determines a well layout that maximizes groundwater temperatures at all extraction wells. Comparing the results from these scenarios demonstrates that hydrogeological conditions can have a significant impact on the optimal well layout. The proposed method is equally applicable to systems with multiple extraction and injection wells and can be extended to various other shallow geothermal applications, such as combined heating and cooling systems.

Keywords: Optimization, Well layout, Heat pump, Groundwater, Adjoint

1. Introduction

The European Union has set itself the goal of being climate neutral by 2050 [1]. This implies the decarbonization of all energy-related sectors, including residential heating and cooling. One of the key technologies to decarbonize this sector are heat pumps [2], as they use renewable resources, are highly efficient and can provide additional flexibility to the electricity system [3]. In particular, shallow geothermal heat pumps are gaining in importance due to their higher efficiency compared to air-water heat pumps [4].

*Corresponding author
Email address: smajil.halilovic@tum.de (Smajil Halilovic)

Nomenclature

Latin letters

$\mathbf{A}$	coefficient matrix of constraints
a, b	coefficients of linear constraints
B	saturated aquifer thickness [m]
$\mathbf{b}$	coefficient vector of constraints
C_{m}	volumetric heat capacity of medium [J/m^{3}K]
C_{w}	volumetric heat capacity of water [J/m^{3}K]
D	feasible area for wells
d	distance [m]
$\mathbf{D}_{\mathrm{mech}}$	tensor of mechanical dispersion [m^2/s]
d_R	regulatory distance [m]
$\mathcal{F}$	residual of equations
f_μ	viscosity relation function [-]
f^{B}	aquifer bottom [m]
G	penalty field
g	inequality constraints
h	hydraulic head [m]
h_{n}	natural groundwater head [m]
$\mathbf{I}$	unity or identity matrix [-]
J	functional of interest
$\hat{J}$	reduced functional of interest
$\mathbf{K}$	tensor of hydraulic conductivity [m/s]
$\boldsymbol{m}$	design/control variables
N	number of heat pumps
N^{cst}	number of constraints
n_{iter}	number of optimization iterations
p	penalty function
P_R, P_T	penalty terms
$\overline{P}_{\mathrm{t}}$	depth integrated heat source/sink terms [W/m^2]
$\mathbf{q}$	Darcy velocity [m/s]
$\overline{Q}$	depth integrated liquid source/sink terms [m/s]
q	pumping rates [m^3/s]
R	restricted area for wells
r	radius of approximate delta function [m]
r^{p}	radius of restricted area [m]
S_0	aquifer storativity [1/m]
T	groundwater temperature [K]
t	time [s]
T^{inj}	temperature of reinjected water [K]
$\boldsymbol{u}$	state variables
V_{norm}	normalization volume [m^3]
$\mathbf{x}^{\mathrm{ext}}$	coordinates of extraction wells [m]
$\mathbf{x}^{\mathrm{inj}}$	coordinates of injection wells [m]
$\mathbf{x}^{\mathrm{p}}$	coordinates of penalty center [m]

Greek letters

α, γ	penalty scaling factors [-]
β_L	longitudinal dispersivity [m]
β_T	transverse dispersivity [m]
$\boldsymbol{\varphi}$	adjoint variables
δ	2D Dirac delta function [1/m^2]
Λ	coefficient of thermal conductivity of liquid [J/mKs]
Λ^s	coefficient of thermal conductivity of solid [J/mKs]
$\boldsymbol{\Lambda}$	tensor of hydrodynamic thermodispersion [W/mK]
Ω	computational domain
$\partial\Omega$	domain boundary
ψ	approximate delta function [1/m^2]
ε	porosity [-]
ε_e	specific yield [-]

Subscripts and superscripts

ext	extraction
inj	injection
in	inflow
min	minimum
i, j	counters

Groundwater heat pumps (GWHPs), along with ground source heat pumps, are one of two main types of geothermal heat pumps. GWHPs are open-loop systems, which means that they use heat directly from the groundwater and, in contrast to closed-loop systems, do not require any additional heat carrier fluid. Residential GWHP systems usually have a single pair of wells in which the groundwater is pumped from the extraction well and, after the energy (heat) exchange, the cooled water is returned into the same aquifer at the injection well. The returned water causes thermal anomalies, so-called thermal plumes, which spread in the aquifer according to the natural groundwater flow direction and can reach neighboring downstream GWHP systems [5]. Potential negative interaction events such as this must be avoided because the efficiency of GWHPs depends significantly on the groundwater temperature [6].

On the other hand, urban areas have high shallow geothermal potential, since ground temperatures are anthropologically elevated by the subsurface urban heat island (SSUHI) effect [7, 8]. Therefore, in addition to being a climate-friendly technology, there is an incentive to install more GWHP systems in urban areas due to the potentially increased efficiency and the need to mitigate further groundwater temperature rise. However, an increased number of GWHPs can lead to negative interactions between neighboring systems. In order to avoid such negative effects, an optimal management of the resource is required [9]. GWHP systems can be carefully positioned in an attempt to minimize any negative interactions, i.e. to maximize the efficiency of all systems, and at the same time to maximize the shallow geothermal potential of a specific region.

A few research studies discuss negative interactions between GWHPs and their connection to the shallow geothermal potential. Attard et al. [10] introduced a new concept to prevent thermal interference between neighboring GWHPs based on thermal protection perimeters, which are defined around existing GWHPs. These protection zones ensure minimum distances between new and existing systems in order to avoid negative interactions. On the other hand, García-Gil et al. [11] proposed a new management policy for GWHPs based on numerical models and a relaxation factor. The factor ensures that part of the geothermal potential is available for future GWHP systems and thus prevents its monopolization. Epting et al. [12] presented a method for evaluating the theoretical and technical shallow geothermal potential on an urban scale. The technical potential is based on the TAP method (Thermal Aquifer Potential) [13], which takes into account the legal and operational framework conditions for GWHPs. However, possible negative thermal interactions between neighboring GWHPs are not part of the TAP method and are therefore only qualitatively discussed in [12]. None of these studies consider any optimization method, but there is a clear need for such methods to maximize the shallow geothermal potential through optimal placement of GWHP systems, i.e. their wells.

In general, well placement is important for a single GWHP system to avoid hydraulic and thermal breakthroughs [14] within the system, but optimal well placement can also be used to reduce negative interactions with neighboring systems. However, while there exist several research studies on the optimization of bore-

hole heat exchanger (BHE) fields [15, 16], there is still a lack of research on the optimization of well layouts for GWHPs. Most of the existing studies only use simulation methods to analyze a few possible spatial patterns of wells. Zhou and Zhou [17] numerically simulated a GWHP with one well doublet using several different spacings between wells (20–100 m) and cooling load variations (± 20%). Gao et al. [18] performed a numerical investigation of four different predefined well configurations of a single GWHP system. Similarly, Lo Russo and Civita [19] compared five exploration scenarios to find a suitable design, including the spatial pattern of extraction and injection wells, for a GWHP serving a large commercial building. All previously described scenario (simulation) based designs of well layouts have two major drawbacks: only inferior designs are found compared to the fully optimized designs, and additional manual work is required for each new system to define suitable scenarios. More recently, Park et al. [20] developed a simulation-optimization model to find optimal pumping rates of a GWHP system. Their approach is based on the coupling of a numerical groundwater simulator with a genetic optimization algorithm. Park et al. [21] further developed this model to determine optimal well locations and pumping rates of a single GWHP. Optimal well locations are found in such a way that the extraction well is fixed and the injection well is optimally selected from a set of predefined locations. The existing methods either evaluate only a relatively small number of predefined well layouts using simulation scenarios [17, 18, 19], or, due to the underlying optimization method, enable optimization over a small number of discrete (predefined) well positions [21]. As a result, possible well layout designs are not fully explored, i.e. only sub-optimal well positions are determined, which can reduce the efficiency and lifespan of GWHPs. Furthermore, research so far has only focused on finding optimal well locations for a single GWHP system, but has not considered the case of multiple GWHPs in order to reduce their mutual negative interactions and thus maximize the geothermal potential of a given area. Therefore, existing methods have several limitations and are not suitable to fully optimize well layouts of GWHP systems, especially in cases where multiple wells need to be optimized simultaneously.

The main objective of this paper is to introduce a new method for optimizing well layouts of GWHP systems that closes the previously identified research gaps. The new method is a significant improvement over existing methods because both a continuous variation and large numbers of well locations can be considered within the optimization procedure. In addition, the newly proposed method can optimize well locations of multiple systems simultaneously, since the number of optimized wells is not a limiting factor. The underlying method is a gradient-based optimization and relies on an efficient computation of gradients using the adjoint approach. As an integral part of this optimization concept, the numerical simulation of the groundwater flow and heat transport is performed using the finite element method (FEM). The applicability of the method is demonstrated using a case study where negative interactions between several neighboring GWHP systems are minimized, i.e. wells are placed to maximize groundwater temperatures at all extraction wells. It should be emphasized that the method can also be directly applied to find optimal well arrangements of individual systems.

The paper is structured as follows. Section 2 describes the methodology, i.e. the new optimization method. Section 3 provides information about the implementation of the method, as well as the selected case study, followed by the results, which are presented and analyzed in Section 4. In Section 5, limitations and possible improvements of the method, including future applications, are discussed. Finally, Section 6 provides conclusions for this work.

2. Methodology

The methodology can be divided into two parts: simulation and optimization. The forward simulation (section 2.1) is a numerical calculation to evaluate a specific well layout, i.e. to calculate the corresponding thermal and hydraulic groundwater conditions. The optimization (section 2.2), on the other hand, finds the best (optimal) well layout for a given objective, such as maximizing the temperatures at the extraction wells.

2.1. Forward simulation model

To analyze the impacts of GWHPs on an aquifer, a forward model describing flow and heat transport in the groundwater (porous media) is required. This simulation model can be formulated as a system of coupled partial differential equations (PDEs), which reads as follows [22]:

$$(BS_0 + \varepsilon_e)\frac{\partial h}{\partial t} + \nabla \cdot (B\mathbf{q}) = \overline{Q}, \tag{1a}$$

$$\mathbf{q} = -\mathbf{K} f_\mu \cdot \nabla h, \tag{1b}$$

$$B = h - f^{\mathrm{B}}, \tag{1c}$$

$$BC_{\mathrm{m}}\frac{\partial T}{\partial t} - \nabla \cdot (B\mathbf{\Lambda} \cdot \nabla T) + BC_{\mathrm{w}}\mathbf{q} \cdot \nabla T = \overline{P}_{\mathrm{t}}. \tag{2}$$

The given PDE system describes 2D vertically averaged, i.e. horizontal, flow and heat transport in an unconfined aquifer. The first set of equations (1) represents flow in porous media, whereas the third PDE (2) represents heat transport in porous media, written here in convective form. All symbols from the PDE system are described in the nomenclature. The physical meaning of the PDEs as well as the modifications and assumptions used in this work are described in the following.

The first PDE (1a) corresponds to the mass conservation law, where the hydraulic head h and the Darcy velocity $\mathbf{q}$ are dependent variables. The aquifer's thickness B is defined as a difference between h and the bottom of the aquifer f^{B}. The term $\overline{Q}$ represents the depth integrated liquid source/sink terms. In this work,

it is assumed that the only source and sink terms correspond with the wells of GWHPs, i.e. $\overline{Q} = \sum_{i=1}^{N} \overline{Q}_i$, where $\overline{Q}_i$ is the source/sink term of the GWHP i, with N the number of GWHPs. Furthermore, it is assumed that each GWHP has two wells: an extraction well (sink term) and an injection well (source term). Wells can be modeled (idealized) with well-type singular point sinks or sources at their locations $\mathbf{x}_i = (x_i, y_i) \in \mathbb{R}^2$ [22]. Based on this, for each GWHP i:

$$\overline{Q}_i = q_i(t)\delta(\mathbf{x} - \mathbf{x}_i^{\mathrm{inj}}) - q_i(t)\delta(\mathbf{x} - \mathbf{x}_i^{\mathrm{ext}}), \tag{3}$$

where $q_i(t)$ is the pumping rate of the GWHP, and "inj" and "ext" stand for injection and extraction, respectively.

The second PDE (1b) represents Darcy's law, which has the same dependent variables as (1a). The PDEs (1a)–(1b) can be solved simultaneously or sequentially by introducing (1b) into (1a). To simplify the computation, the second approach is followed in this work, where the unknown h is computed first and thereafter $\mathbf{q}$ is obtained directly from (1b). Moreover, to linearize (1a) and reduce computational costs, the effect of wells on the saturated aquifer's thickness B is neglected, i.e. it is assumed that B only depends on the natural groundwater head h_{n}:

$$B = h_{\mathrm{n}} - f^{\mathrm{B}}. \tag{4}$$

This is an acceptable assumption since the GWHP systems considered in this work are relatively small and have low pumping rates, which leads to low groundwater depression cones. It should be noted that the effects of wells on the state h are still taken into account in the PDEs, and are only neglected in the term B used for vertical averaging.

The third PDE (2) describes the heat transport in a two-phase (liquid and solid) medium, i.e. groundwater. The main dependent variable here is the groundwater temperature T, whereas other terms are constant parameters or solutions from the previous PDEs. The second term in (2) describes the heat conduction and dispersion, and the third term the thermal advection, respectively. The parameter $\mathbf{\Lambda}$ in the second term is the hydrodynamic thermal dispersion, which can be calculated using the following equations [22]:

$$\mathbf{\Lambda} = (\varepsilon\Lambda + (1-\varepsilon)\Lambda^s)\mathbf{I} + C_{\mathrm{w}}\mathbf{D}_{\mathrm{mech}}, \tag{5}$$

$$\mathbf{D}_{\mathrm{mech}} = \beta_T\|\mathbf{q}\|\mathbf{I} + (\beta_L - \beta_T)\frac{\mathbf{q}\otimes\mathbf{q}}{\|\mathbf{q}\|}, \tag{6}$$

with symbols' descriptions given in the nomenclature. The term $\overline{P}_{\mathrm{t}}$ in (2) represents vertically averaged heat sink/source terms. In this work, it is assumed that the only heat sinks/sources correspond with the wells of GWHPs, i.e. $\overline{P}_{\mathrm{t}}$ is given by:

$$\overline{P}_{\mathrm{t}} = \sum_{i=1}^{N} q_i(t)C_{\mathrm{w}}[T_i^{\mathrm{inj}}(t) - T]\delta(\mathbf{x} - \mathbf{x}_i^{\mathrm{inj}}), \tag{7}$$

where $T_i^{\text{inj}}(t)$ is the temperature of re-injected water at the injection well of GWHP i. It should also be noted that since the energy exchange only takes place at injection wells of GWHPs, only the injection wells appear as heat sinks in (7).

The flow PDEs (1) and the heat transport PDE (2) are coupled only in one direction. Hence, they can be solved sequentially, first the flow problem, and then the heat problem. Strictly speaking this is not realistic as the water density and hydraulic conductivity also depend on the temperature of the groundwater. However, neglecting these dependencies simplifies the problem significantly and is a reasonable assumption for the considered application since temperature differences occur over a small range of approximately 5K [23]. Finally, it should be emphasized that in this initial work only the steady state is considered within the optimization process. Thus, all the time dependent components in the previously described system of PDEs are discarded. This means that the PDEs (1a) and (2) take the following form:

$$\nabla \cdot (B\mathbf{q}) = \overline{Q}, \tag{8}$$

$$-\nabla \cdot (B\boldsymbol{\Lambda} \cdot \nabla T) + BC_{\text{w}}\mathbf{q} \cdot \nabla T = \overline{P}_{\text{t}}, \tag{9}$$

whereas (1b) remains the same.

2.2. Optimization

The optimization objective is to maximize the groundwater temperatures at extraction wells of GWHPs, since the efficiency of GWHPs increases with increasing groundwater temperature at those wells. The underlying problem can be described as a PDE-constrained optimization (PDECO) problem, since the groundwater flow and heat transport are modeled with the previously described system of PDEs. In general, PDECO problems can be formulated as follows:

$$\min_{\boldsymbol{u},\boldsymbol{m}} \quad J(\boldsymbol{u},\boldsymbol{m}), \tag{10a}$$

$$\text{subject to} \quad \mathcal{F}(\boldsymbol{u},\boldsymbol{m}) = 0, \tag{10b}$$

$$g(\boldsymbol{u},\boldsymbol{m}) \leq 0, \tag{10c}$$

where $J(\boldsymbol{u},\boldsymbol{m}) \in \mathbb{R}$ is the functional of interest and is used to describe mathematically the objective of the optimization, $\boldsymbol{u}$ are the state variables that are the solution of a PDE or a system of PDEs represented in a residual form by $\mathcal{F}(\boldsymbol{u},\boldsymbol{m}) = 0$, $\boldsymbol{m}$ are the design/control variables, and g any additional inequality constraints on controls and/or states.

The problem (10) can be solved in two ways: using full space or reduced space methods [24]. In the former, states and controls are considered both as optimization variables within the optimization algorithm (solver) and changed directly and simultaneously in each optimization iteration. In the latter, the mapping

$\boldsymbol{m} \mapsto \boldsymbol{u}(\boldsymbol{m})$, which is implicitly defined by the PDE constraint(s) $\mathcal{F}(\boldsymbol{u}, \boldsymbol{m}) = 0$, is used to obtain the reduced problem [24]:

$$\min_{\boldsymbol{m}} \qquad \hat{J}(\boldsymbol{m}) := J(\boldsymbol{u}(\boldsymbol{m}), \boldsymbol{m}), \tag{11a}$$

$$\text{subject to} \qquad g(\boldsymbol{u}(\boldsymbol{m}), \boldsymbol{m}) \leq 0, \tag{11b}$$

where $\hat{J}(\boldsymbol{m})$ is termed the reduced functional of interest. The reduced problem is suitable for use with the adjoint approach for computing functional gradients. In this work, a gradient-based optimization is used together with the adjoint approach, which is the most efficient technique of computing the required gradients in each optimization iteration [25].

In each iteration, gradient-based optimization algorithms require computation of the gradient of the functional with respect to the control variables:

$$\frac{\mathrm{d}\hat{J}}{\mathrm{d}\boldsymbol{m}} = \frac{\mathrm{d}J(\boldsymbol{u}(\boldsymbol{m}), \boldsymbol{m})}{\mathrm{d}\boldsymbol{m}} = \frac{\partial J}{\partial \boldsymbol{m}} + \frac{\partial J}{\partial \boldsymbol{u}} \frac{\mathrm{d}\boldsymbol{u}}{\mathrm{d}\boldsymbol{m}}. \tag{12}$$

The partial derivatives $\partial J/\partial \boldsymbol{m}$ and $\partial J/\partial \boldsymbol{u}$ can be computed analytically and are, thus, computationally cheap to evaluate. On the other hand, the derivative $\mathrm{d}\boldsymbol{u}/\mathrm{d}\boldsymbol{m}$ is computationally expensive for high-dimensional states $\boldsymbol{u}$ and controls $\boldsymbol{m}$. In general, the discretized state space is high-dimensional in PDECO problems, whereas the dimension of the control space depends on the number and type (a constant, or a spatially or time-varying function) of controls. In the adjoint approach, the direct computation of $\mathrm{d}\boldsymbol{u}/\mathrm{d}\boldsymbol{m}$ is avoided and the functional gradient is obtained as follows [24]:

$$\frac{\mathrm{d}\hat{J}}{\mathrm{d}\boldsymbol{m}} = \frac{\partial J}{\partial \boldsymbol{m}} - \boldsymbol{\varphi}^* \frac{\partial \mathcal{F}}{\partial \boldsymbol{m}}, \tag{13}$$

where $\boldsymbol{\varphi}$ are the adjoint variables, and * denotes the Hermitian operator. The adjoints are obtained from the adjoint equation:

$$\frac{\partial \mathcal{F}}{\partial \boldsymbol{u}}^* \boldsymbol{\varphi} = \frac{\partial J}{\partial \boldsymbol{u}}^* . \tag{14}$$

Therefore, the computation of the functional gradient involves two steps: solving (14) for the adjoint variables and using the obtained values in (13). Since the adjoint equation does not contain derivatives with respect to controls and is a linear PDE, the computational effort for its solution is independent of the size of the control and if implemented efficiently is generally less or as expensive as solving the forward problem described by $\mathcal{F}$. As a result, the adjoint approach enables an efficient computation of functional gradients independent of the dimension of the control variables.

2.2.1. Optimization variables and the functional of interest

The main objective of the optimization procedure is to design the placement of the GWHP systems, i.e. their extraction and injection wells, in a way that the efficiency of all GWHPs is maximized and

all regulatory conditions are met. Therefore, the **control optimization variables** are the Cartesian coordinates (positions) of wells: $\mathbf{x}_i^{\text{ext}} = (x_i^{\text{ext}}, y_i^{\text{ext}}) \in \mathbb{R}^2$ represents the extraction well coordinates of the heat pump i and $\mathbf{x}_i^{\text{inj}} = (x_i^{\text{inj}}, y_i^{\text{inj}}) \in \mathbb{R}^2$ represents the injection well coordinates of the same heat pump. All control variables can be described using the following vector:

$$\boldsymbol{m} = [x_1^{\text{ext}}, ..., x_N^{\text{ext}}, y_1^{\text{ext}}, ..., y_N^{\text{ext}}, x_1^{\text{inj}}, ..., x_N^{\text{inj}}, y_1^{\text{inj}}, ..., y_N^{\text{inj}}]^T. \tag{15}$$

The **state optimization variables** are the solutions of the governing PDEs, i.e. the hydraulic head h, Darcy velocity $\mathbf{q}$ and the groundwater temperature T.

The optimization goal is to maximize the groundwater temperatures at all extraction wells. Thus, the corresponding functional of interest J_0 reads as follows:

$$J_0(\boldsymbol{u}, \boldsymbol{m}) = \sum_{i=1}^{N} T(\mathbf{x}_i^{\text{ext}}) = \sum_{i=1}^{N} \int_\Omega T(\mathbf{x}) \cdot \delta(\mathbf{x} - \mathbf{x}_i^{\text{ext}}) \, \mathrm{d}\Omega. \tag{16}$$

The point evaluation of the function T, i.e. sampling of the groundwater temperature field at the extraction well, can be formulated as an integral of the product of the function T and the corresponding 2D Dirac delta function. In this work, the short notation for the point evaluations of functions (states) will be used from now on, but the implementation is based on the previously described multiplication with delta functions.

2.2.2. Optimization constraints

The underlying PDECO problem includes control constraints, which are based on the regulations and physical conditions when placing (installing) new GWHP systems. The first set of constraints corresponds to the fact that the wells of a GWHP can be placed only inside a plot (property) that belongs to the owner of that GWHP. In addition, approval regulations for new systems usually stipulate a minimum distance between the wells and the plot boundaries. For instance, this distance is 3 meters in Bavaria (Germany) [26], where the considered case study is located. Thus, for each GWHP i the constraints state that both wells, extraction and injection, must be restricted to the feasible area D_i that corresponds to the plot area excluding a minimum-distance buffer zone:

$$\mathbf{x}_i^{\text{ext}}, \mathbf{x}_i^{\text{inj}} \in D_i, \quad \forall i \in \{1, ..., N\}. \tag{17}$$

In the case of idealized rectangular plots aligned with the coordinate system, these constraints would take a particularly simple form as upper and lower bounds on controls. However, in this work, a more realistic and general case with convex plots is considered. The constraints are then formulated as follows:

$$g_i^j(x_i^w, y_i^w) = a_{i,1}^j x_i^w + a_{i,2}^j y_i^w \leq b_i^j, \quad \forall i \in \{1, ..., N\}, \, \forall j \in \{1, ..., n_i\}, \tag{18}$$

where w stands for extraction or injection, i.e. $w \in \{\text{ext}, \text{inj}\}$; i is the counter for plots (GWHPs); j counts the linear segments of the plot boundary, assumed to be a polygon; n_i is the total number of boundary

segments for plot i; $a_{i,1}^j$, $a_{i,2}^j$, b_i^j are the coefficients of the linear inequality constraint that corresponds to the boundary segment j of plot i. These constraints can be also written in matrix form:

$$\mathbf{A}\boldsymbol{m} \leq \mathbf{b}, \tag{19}$$

where the matrix $\mathbf{A}$ contains the coefficients $a_{i,1}^j$ and $a_{i,2}^j$, and the vector $\mathbf{b}$ the coefficients b_i^j. The total number of constraints in (18), N_1^{cst}, depends on the number of segments of plot boundaries and is given as:

$$N_1^{\text{cst}} = \sum_{i=1}^{N} n_i. \tag{20}$$

The coefficients in (18) are derived using analytical formulae and geometric relations, as described in Appendix A.

The second set of constraints corresponds to regulation over the minimum distance between wells of the same GWHP system. The injection well is usually placed downstream and far enough from the extraction well to avoid hydraulic and thermal breakthroughs [14]. Breakthroughs reduce the efficiency of GWHPs because the altered groundwater circulates back to the extraction well [27]. For this reason, there is usually a defined minimum distance between two wells of a system. For example, in Bavaria, Germany, this distance is 10 meters according to current best practice in local water protection authorities. The corresponding constraints can be defined as follows:

$$d(\mathbf{x}_i^{\text{ext}}, \mathbf{x}_i^{\text{inj}})^2 = (x_i^{\text{ext}} - x_i^{\text{inj}})^2 + (y_i^{\text{ext}} - y_i^{\text{inj}})^2 \geq d_{\min}^2, \quad \forall i \in \{1, ..., N\}, \tag{21}$$

where d is the distance function and $d_{\min} = 10$ [m] is the predefined minimum distance. The total number of these control constraints is equal to the number of considered GWHPs, i.e. $N_2^{\text{cst}} = N$.

The regulations also specify minimum distances between GWHP wells and existing objects on a property, such as a house or a garage. The wells cannot be placed within such objects and the minimum distance provides a buffer zone that is necessary from a safety and technical point of view. This regulatory distance d_R is 3 meters [26] in the area of interest (see section 3.1). The corresponding constraints can be summarized as follows:

$$\mathbf{x}_i^{\text{ext}}, \mathbf{x}_i^{\text{inj}} \notin R_i^j, \quad \forall i \in \{1, ..., N\}, \forall j \in \{1, ..., r_i\}, \tag{22}$$

where R_i^j is the restricted area j for wells within the plot i, which is for example a house and its surrounding 3-meter buffer zone; r_i the number of restricted areas in the plot i. Figure 1 shows an example plot with a restricted area and minimum-distance buffer zones. The control constraints in (22) cannot be mathematically formulated as convex linear constraints, such as (18), even when the restricted areas R_i^j are convex polygons. For this reason, these constraints are integrated into the optimization problem via penalty terms, as explained in the following section.

Finally, it should be noted that if the order of installation of GWHPs is defined, i.e. there are some existing GWHPs in the area and the new ones should be optimally placed accordingly, an additional set

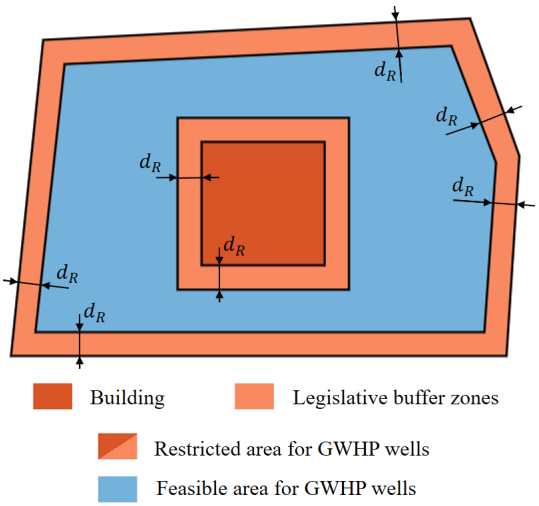


Figure 1: Example of a plot with one building and the corresponding buffer zones ($d_R = 3$ m).

of constraints is required. These constraints correspond to regulations over negative interference between neighboring GWHPs. The details of such constraints and how they can be included in the optimization are given in Appendix B, but they are not considered further in the present study.

2.2.3. Penalty terms

In general, penalty terms (functions) can be used to convert constrained optimization problems into unconstrained ones or to replace only a certain number of constraints. These functions are added to the original objective function and are formulated in such a way that they become zero if the corresponding constraint is met, or otherwise take a positive value in the case of a minimization problem [28]. In the PDECO framework, the penalty functions can be used to replace state constraints or control constraints that are difficult to express in a suitable form for the selected optimization algorithm and/or its software implementation.

Since the control constraints (22) cannot be formulated mathematically as convex linear constraints, they are replaced by penalty functions. The corresponding penalty term P_R, which is added to the functional of interest (16), contains penalty functions for the positions of all extraction and injection wells:

$$P_R = \alpha \cdot \sum_{i=1}^{N} \left(p(\mathbf{x}_i^{\text{ext}}) + p(\mathbf{x}_i^{\text{inj}}) \right), \tag{23}$$

where p denotes the penalty function, and α is a penalty scaling factor that determines how severely the objective will be penalized if the constraints are not met. The penalty function p should be positive if the well under consideration lies within one of the restricted areas R_i^j and otherwise be zero. In this work, the

functions p are defined as a point evaluation of a predefined penalty field:

$$p(\mathbf{x}_i) = \int_{\Omega} G(\mathbf{x}) \cdot \delta(\mathbf{x} - \mathbf{x}_i)\, \mathrm{d}\Omega, \tag{24}$$

where $G(\mathbf{x})$ is the penalty field constructed using the restricted areas R_i^j. The penalty field is defined as follows:

$$G(\mathbf{x}) = \begin{cases} 0 & \text{if} \quad \mathbf{x} \notin R_i^j, \quad \forall i \in \{1, ..., N\}, \forall j \in \{1, ..., r_i\} \\ 1 + \cos\left[\frac{d(\mathbf{x}, \mathbf{x}_{i,j}^{\mathrm{p}})}{r_{i,j}^{\mathrm{p}}} \cdot \frac{\pi}{2}\right] & \text{if} \quad \mathbf{x} \in R_i^j, \end{cases} \tag{25}$$

where $\mathbf{x} = (x, y) \in \Omega$ is an arbitrary point in the domain Ω; d the distance function from (21); $\mathbf{x}_{i,j}^{\mathrm{p}}$ and $r_{i,j}^{\mathrm{p}}$ are the penalty center and the radius of the corresponding restricted area R_i^j, respectively. The penalty field G for an example restricted area is depicted in Figure 2. The idea behind this particular choice of shape for G is that the more a well is within a restricted area, the larger the penalty term and, conversely, the penalty should be smaller the closer the well is to the boundary of the area. This leads to a non-zero gradient, which is important for the gradient-based optimization approach. The radii $r_{i,j}^{\mathrm{p}}$ are selected as the maximum distance between any point belonging to the corresponding area R_i^j and its penalty center $\mathbf{x}_{i,j}^{\mathrm{p}}$. This ensures that the minimum value of $G(\mathbf{x})$ inside restricted areas is $1 + \cos(\pi/2) = 1$. On the other hand, the selection of the centers $\mathbf{x}_{i,j}^{\mathrm{p}}$ is a non-trivial task, since it depends on the relative positions of the restricted areas R_i^j and the corresponding plots D_i. The centers must be chosen in such a way that the points representing the well positions are not "trapped" in a restricted area during the optimization iterations. This type of situation is depicted in Figure 3, where the well i cannot escape the restricted area anymore and reach the feasible part of the domain. Therefore, a distinction is made between three baseline scenarios, as depicted in Figure 4, when selecting penalty centers:

1. the restricted area R_i^j overlaps with only one edge (boundary section) of the plot D_i: the penalty center corresponds to the middle point of overlapping section of that edge;
2. the restricted area R_i^j overlaps with exactly two edges of the plot D_i, including the corner of the plot that is between those two edges: the penalty center corresponds to that particular corner;
3. all other cases: the penalty center corresponds to the geometrical centroid of R_i^j.

These baseline scenarios are usually sufficient to cover many cases, but also provide the general concept for selecting penalty centers in all other cases.

It should be emphasized that by combining penalty functions for restricted areas and inequality constraints for convex plots, any type of plot geometry can be defined. For example, if the original plots are non-convex, they can be converted to convex hulls first and then additional restricted areas can be defined to cover the difference between the original plots and the new (convex) ones. This is important because in the real world, plots have many different geometries, including non-convex ones.

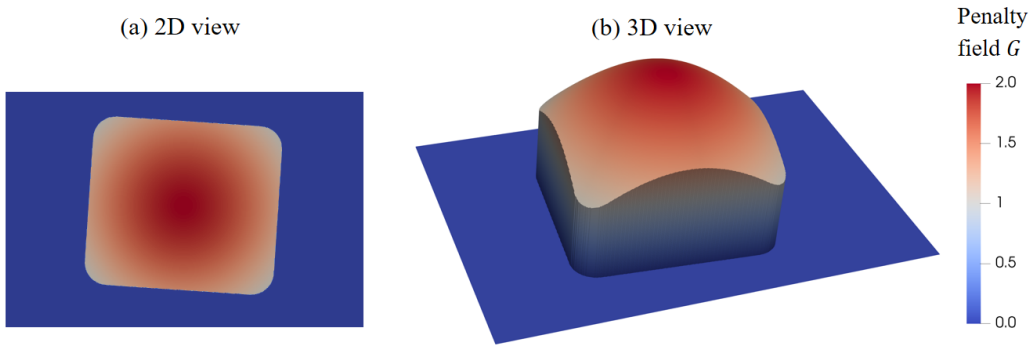


Figure 2: Penalty field for an example restricted area plotted in 2D (a) and 3D (b). If a well is placed in the feasible part (blue color), the penalty field G is 0, otherwise the penalty has a positive value if a well is within the restricted area (red colors).

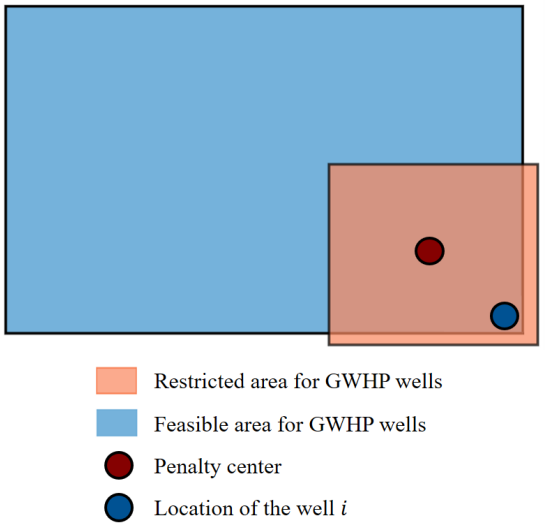


Figure 3: Example of improper selection of a penalty center. The well i cannot reach the feasible area because of the selected position of the penalty center and the underlying shape of the penalty functions.

Finally, it should be noted that the penalty factor α is usually applied in an iterative way. The iterative optimization procedure means that α is increased at the end of each "outer" iteration, i.e. after the optimization algorithm has converged or reached the predefined number of optimization iterations. The solution from the previous outer iteration is used as the starting point for the next iteration. The whole procedure starts with a relatively small value of α and ends when α is considered to be sufficiently large. In general, this iterative approach should help to improve the convergence of optimization algorithms and ideally has the same solution as the original optimization problem, which includes constraints instead of penalties [28]. Also in this work, an iterative optimization with increasing penalty factors is applied (see section 3).

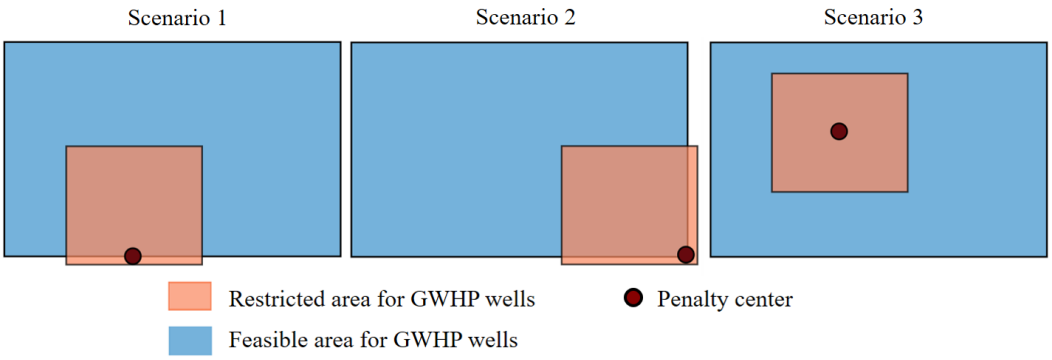


Figure 4: Baseline scenarios for the selection of penalty centers.

2.2.4. Approximated delta functions

The Dirac delta functions are present in two places in the underlying PDECO problem: in the representation of wells, i.e. sink and source terms in PDEs, as well as in the sampling of functions (states and penalty fields), such as the evaluation of the groundwater temperature at extraction wells. The delta function is a non-smooth function and is therefore problematic for gradient-based optimization, which requires information about gradients in each iteration. One approach to address this problem is to replace the delta function with a smooth approximation. A similar approach is used in [29] to represent production wells of a deep geothermal system. In other energy-related applications, such as the layout optimization of wind [30] and tidal turbines [31], the approach of representing the corresponding turbines with approximate smooth functions is already well established. These smooth approximations are usually based on exponential functions and are often referred to as bump functions. The one used in this work is depicted in Figure 5 and defined as follows:

$$\delta(\mathbf{x} - \mathbf{x}_i) \approx \psi(x, y, x_i, y_i) = \mathrm{e}^{-\frac{(x-x_i)^2+(y-y_i)^2}{r^2}}, \tag{26}$$

where $\mathbf{x}_i = (x_i, y_i)$ is the center of the bump function ψ and r its radius. The radius $r = 0.1$ [m] is chosen based on the well dimensions of real GWHPs. For this reason, it can be argued that the well representation in this work is actually more realistic than the usual use of single point sources for wells. Finally, the volume V_{norm} below the surface of the function ψ must be used to normalize the values of the "smoothed" delta function:

$$V_{\text{norm}} = \int_{-\infty}^{\infty} \int_{-\infty}^{\infty} \psi(x, y, x_i, y_i)\, \mathrm{d}x\mathrm{d}y = r^2\pi. \tag{27}$$

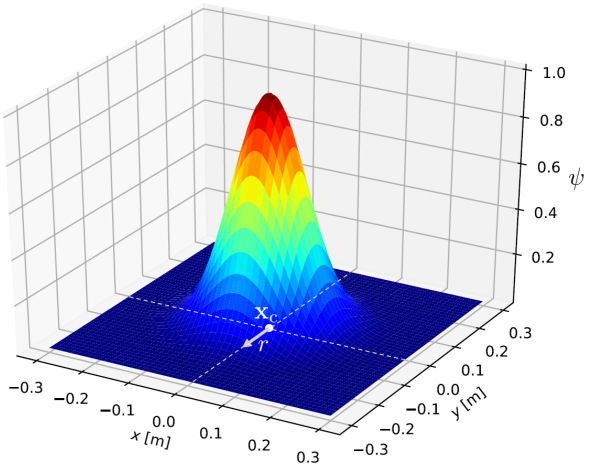


Figure 5: Smooth approximation ψ of the Dirac delta function with center $\mathbf{x}_c = (0, 0)$ and radius $r = 0.1$ [m].

2.2.5. Problem formulation

Based on the previous definitions of constraints, penalty functions and the functional of interest, the optimization problem reads as follows:

$$\min_{\boldsymbol{m}} \quad -\hat{J}_0(\boldsymbol{m}) + P_R(\boldsymbol{m}), \tag{28a}$$

$$\text{subject to} \quad g_1(\boldsymbol{m}) \leq 0, \tag{28b}$$

$$g_2(\boldsymbol{m}) \leq 0, \tag{28c}$$

where $\hat{J}_0(\boldsymbol{m}) = J_0(\boldsymbol{u}(\boldsymbol{m}), \boldsymbol{m})$ is the reduced form of the functional of interest J_0 defined in (16); $P_R(\boldsymbol{m})$ the penalty term from (23); $g_1(\boldsymbol{m}) = \mathbf{A}\boldsymbol{m} - \mathbf{b}$ corresponds to the linear inequality constraints (19), and $g_2(\boldsymbol{m})$ to the minimum distance constraints (21). Since the sense of optimization is changed from maximization in (16) to minimization in (28), a negative sign is introduced in front of $\hat{J}_0$. The underlying problem represents a PDECO problem with control constraints.

2.2.6. Problem initialization

The underlying optimization problem is non-convex, which means that gradient-based algorithms converge towards a local optimum. Therefore, the selection of the initial optimization candidate is important, as those that are close to the global optimum are more likely to converge to it. Figure 6 shows the multi-start initialization strategy used in this work to achieve the global optimum or to come sufficiently close to it. In the first step, different combinations of initial GWHP well positions, i.e. samples, are generated using the Latin Hypercube Sampling (LHS) method [32]. The LHS implementation in Python [33] provides only lower and upper limits on sampling points, i.e. well coordinates in this case. Therefore, the obtained LHS samples are in general not feasible, since they do not satisfy the optimization constraints (17), (21) and (22). In the

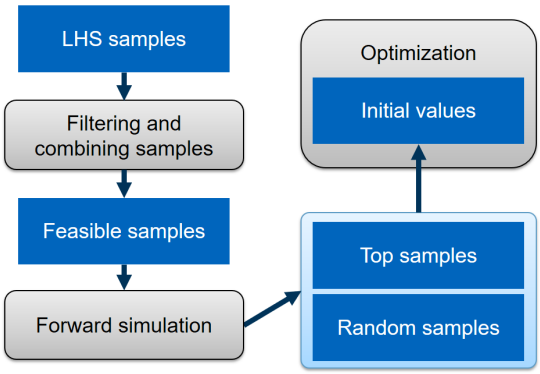


Figure 6: Multi-start initialization strategy.

second step, the LHS samples are filtered and mutually combined to obtain feasible samples that meet all optimization constraints. The feasible samples are combinations of well positions that are within feasible areas (plots), with sufficient spacing between wells of the same GWHP and outside of restricted areas. In addition, for each well pair, it is required that the injection well is located downstream of the extraction well for the samples to be considered feasible. In the third step, a forward simulation is carried out for each feasible sample and the functional of interest (16) is computed. Based on the value of this functional, all samples are sorted in ascending order. Finally, two smaller sets of feasible samples are selected for the initialization: the top-most samples, which have the smallest functional values, and a set of random samples. In addition to improving the optimal solution, these different starting points are also used to investigate the influence of the initialization on the optimization process. To adequately explore the design space, 1000 feasible samples are generated in this work and then the top 10 top samples and 5 random samples are used for initialization.

3. Implementation

The forward simulation model is implemented in Firedrake [34], which is an open-source tool for solving PDEs using the finite element method (FEM). Firedrake provides high-level abstractions for defining and solving PDE problems in the Python environment. Further advantages are MPI parallelization and compatibility with dolfin-adjoint [35], which can automatically provide adjoint solution fields based purely on the forward numerical model defined in Firedrake. These two tools are used to implement and solve the PDECO problem (28), where dolfin-adjoint provides interface to optimization algorithms. The implemented forward model is verified against corresponding simulation results obtained using FEFLOW [22, 36], an established commercial software package for groundwater simulations. The Sequential Least SQuares Programming (SLSQP) algorithm [37] and its implementation in the SciPy Python library [38] are used to solve the underlying optimization problem. The penalty factor α is applied iteratively as described previously

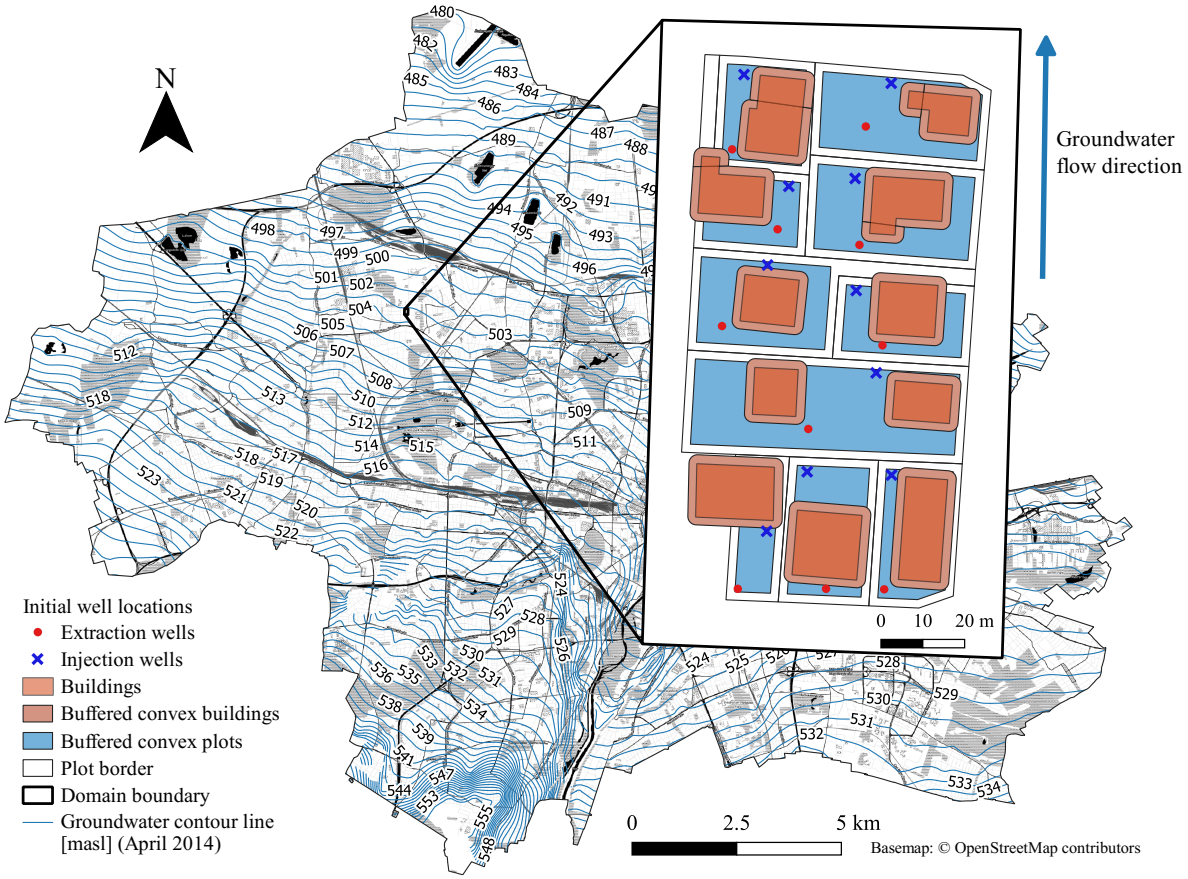


Figure 7: Location of the case study domain in Munich with a detailed view of the relevant features.

in section 2.2.3, using the following increasing values: 0, 0.1, 1, 10, 100. For each of the five α values, the maximum number of optimization iterations is set to 50.

3.1. Case study

The method is applied in a 1.3-hectare study area in the City of Munich, Germany. Munich offers an exceptional hydro-geological database acquired in predecessor projects, namely GEPO and GeoPot [39]. As shown in Figure 7, the study area comprises 10 plots of land with a typical building structure of 11 single-family detached houses. With the simplifying assumption that the heat demand of every plot can be supplied and re-injected by one extraction and one injection well, the optimal positions of 10 well pairs are determined in the case study. Geologically, the case study area is situated in the so-called Munich Gravel Plain which provides favorable conditions for the thermal use of groundwater [13]. Generally, the fluvio-glacial sandy gravels have a high hydraulic conductivity and they host a productive shallow aquifer (cf. Figure 8). Beneath the Quaternary gravels, intersecting Tertiary sandy, silt and clay layers confine the aquifer to the bottom [40]. The study area was selected because it offers favorable hydro-geological

conditions and a low depth to groundwater of around 3.5 m that would additionally support an economical installation of groundwater heat pumps. The elongated shape from south to north was chosen for this test case so as to trigger negative thermal interactions between injection and extraction wells of potential systems, as groundwater flow is also directed towards the North, and thus to demonstrate the value of an PDE-constrained optimization based design approach.

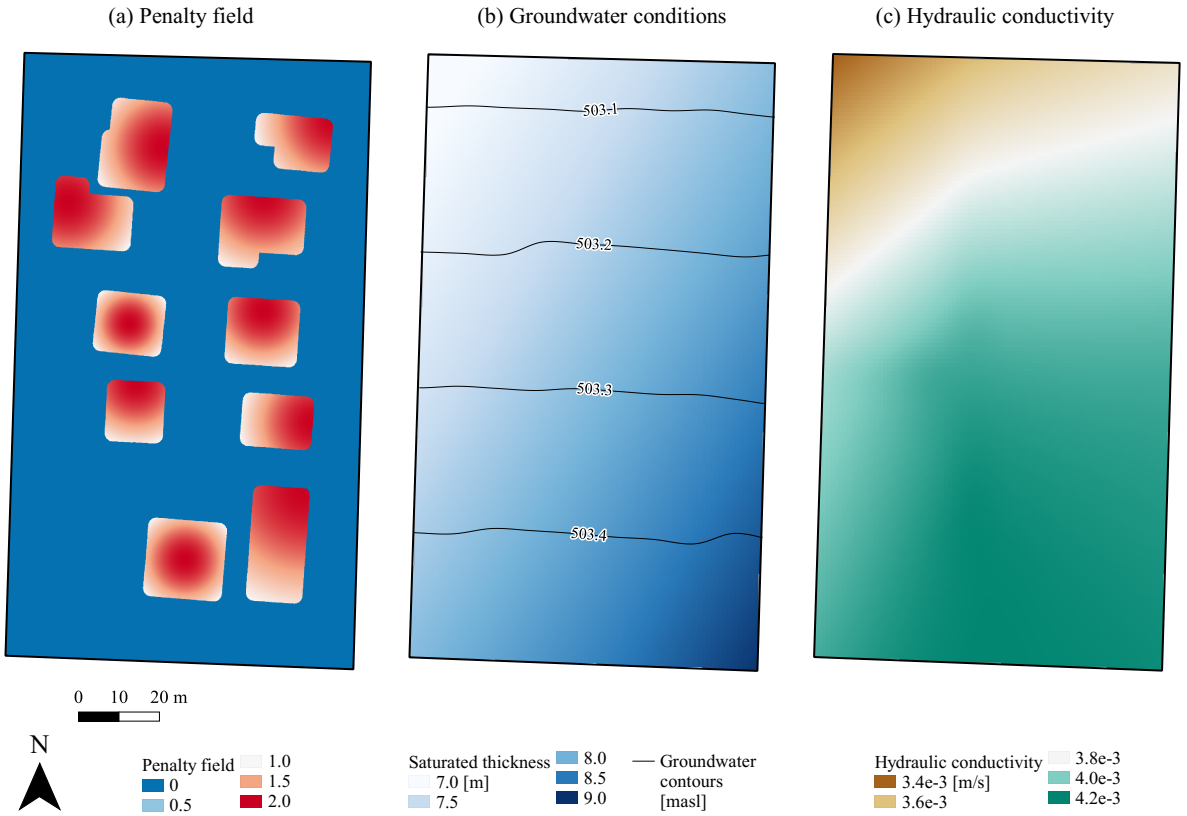


Figure 8: Case study domain with penalty field, initial groundwater conditions and hydraulic conductivity.

Figure 8a shows the penalty field for restricted areas in the study case (see section 2.2.3). In addition, the saturated thickness of the Quaternary aquifer, the groundwater contours and the hydraulic conductivity are depicted in Figure 8b and Figure 8c, respectively. The aquifer basis was derived by geostatistical relief modeling of the entire Munich Gravel Plain [41]. Within the domain of the case study, a northward directed groundwater flow with a homogeneous hydraulic gradient of 2.8 per mill is present. The saturated thickness is computed by subtracting the base of the Quaternary aquifer from the shown groundwater table, which was measured at mean low water conditions in April 2014. As observable in Figure 7, this represents the common regional conditions in the Northwest of Munich. The saturated thickness decreases from 9 m to 7

Table 1: Constant pumping rates and the heating power of the domain's 10 GWHP systems.

Plot ID	1	2	3	4	5	6	7	8	9	10
Pumping rate [L/s]	0.65	0.49	0.42	1.03	0.84	0.51	0.76	0.56	0.58	0.44
Heating power [kW]	13.65	10.29	8.82	21.63	17.64	10.71	15.96	11.76	12.18	9.24

m towards the Northwest. Thus, the domain offers slightly higher values compared to the median thickness of 6.3 m over the entire city area. The hydraulic conductivity of the domain was derived by an interpolation of pumping test data and represents the highly conductive and homogeneous gravels of the area [42].

To solve the underlying PDE system that describes the heat transport and groundwater flow in the aquifer, the pumping rates of all 10 GWHPs have to be defined. These are calculated from the annual heating demand and assuming 2400 full load hours per year, as well as a constant annual performance factor of 4 and a temperature difference of -5 K at the injection well. The heating demand of each system, i.e. each building, is estimated using an open source tool UrbanHeatPro [43]. The obtained values of pumping rates and the heating power are summarized in Table 1, with the system labels corresponding to those in Figure 9.

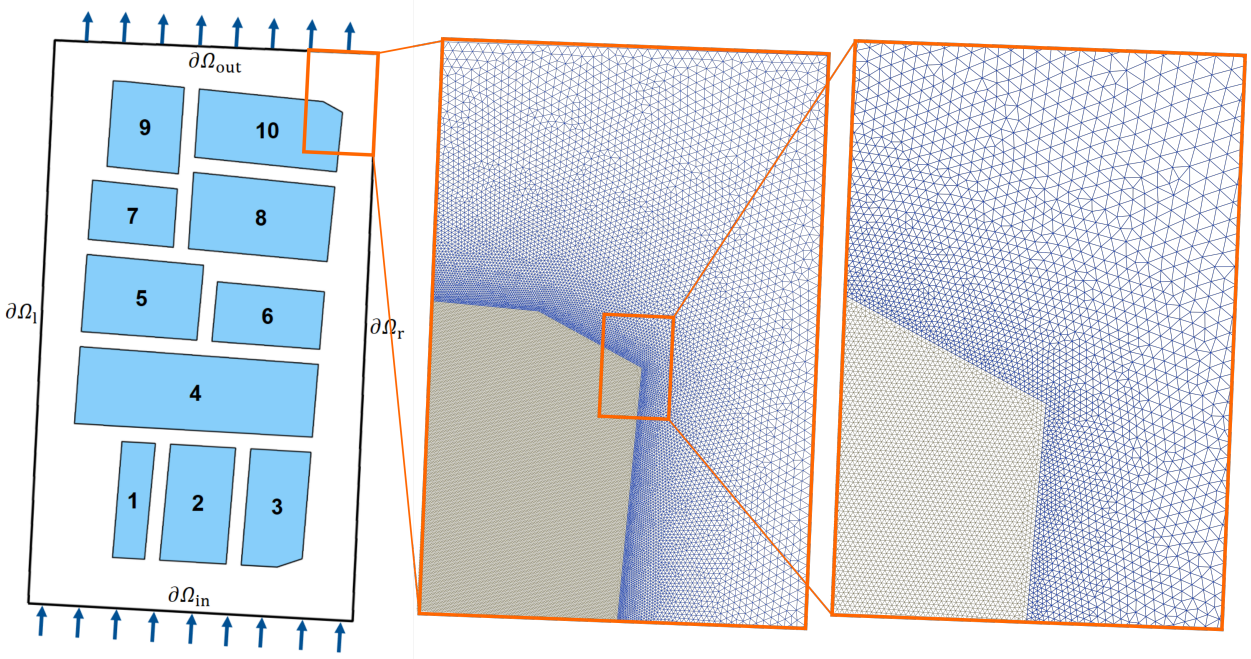


Figure 9: Case study area with its boundary and GWHP (plot) labels and sections of the corresponding finite element mesh.

For the numerical modelling of the groundwater source, the domain is discretized with approximately $3 \cdot 10^6$ triangular elements using the open source mesh generator Gmsh [44]. Element sizes range from 0.08 m within plots to 3 m further away from plots, as shown in Figure 9. The fine mesh resolution within

plots is necessary because the wells can be placed anywhere in plots during the optimization iterations, and the approximated delta functions representing wells require a relatively fine spatial discretization. Mesh sensitivity testing shows that the element size of 0.08 m is required to generate an acceptable discretization error for the delta functions and the application considered in this work. Piece-wise linear finite element basis functions (P1) are used for all state variables, as they provide sufficiently accurate results and are computationally less expensive than higher-order basis functions. For the interpolation of the smooth delta functions (cf. (26)), piece-wise quadratic basis functions (P2) prove to be sufficient.

As shown in Figure 9, Dirichlet type boundary conditions were assigned at the upstream $\partial\Omega_{\text{in}}$ and downstream $\partial\Omega_{\text{out}}$ border to represent a constant hydraulic head at 503.492 masl for inflow and 503.064 masl for outflow, respectively. At the remaining borders parallel to the groundwater streamlines, no boundary condition was assigned, which corresponds to a Neumann type boundary condition without fluid flux [22]. Extraction and injection wells are hydraulically represented through single node sink and source terms approximated by smooth delta functions (see section 2.2.4), where abstraction and injection rates are always equal within one well pair. Due to the assumption of a constant natural groundwater temperature, the heat transport simulation can be solved with only one Dirichlet type boundary condition at the upstream border $\partial\Omega_{\text{in}}$. The assigned temperature depends on the optimization scenario, as described in section 3.2. The thermal impact of the injection wells is represented with an assignment of 5°C to the temperature of re-injected water at those wells T_i^{inj} (cf. (7)). Normally, injection well temperatures are assigned based on extraction well temperatures by subtracting a constant predefined temperature difference. However, since the extraction well temperatures are changing with the well positions during the optimization, it is assumed for the sake of simplicity that the injection well temperatures T_i^{inj} are independent of the extraction well temperatures. The predefined value of 5°C is based on the expected average extraction well temperatures of 10°C (see section 3.2) and a temperature difference of -5 K.

3.2. Optimization scenarios

Two optimization scenarios are used to demonstrate the ability of the optimization process to produce suitable results based on different hydro-geological conditions, as well as to show how these conditions affect the optimal well layout. These two scenarios differ in the natural temperature of the inflowing groundwater. In the first scenario, the groundwater temperature at the inflow boundary of the domain is set to be constant, i.e. $T_{\text{in}} = 10°\text{C}$. In the second scenario, the groundwater temperature is higher in the middle of the inflow boundary and lower at its edges:

$$T_{\text{in}}(\mathbf{x}) = T_{\text{in}}^{\min} + \Delta T_{\text{in}} \cdot \cos\left[\frac{d(\mathbf{x}, \mathbf{x}_{\text{in}})}{r_{\text{in}}} \cdot \frac{\pi}{2}\right], \quad \mathbf{x} \in \partial\Omega_{\text{in}}, \tag{29}$$

where $T_{\text{in}}^{\min} = 8°\text{C}$ is the temperature at the boundary edges, $\Delta T_{\text{in}} = 4°\text{C}$ the temperature difference between the maximum and minimum temperature at the boundary, $d(\mathbf{x}, \mathbf{x}_{\text{in}})$ distance between a point $\mathbf{x}$

at the inflow boundary $\partial\Omega_{\text{in}}$ and its geometric center $\mathbf{x}_{\text{in}}$, and r_{in} the "radius" of the boundary, i.e. the distance between its center point and one of the edges. The groundwater temperature at the boundary center corresponds to the maximum temperature of 12°C. Conceptually, optimization scenario 2 represents the case where groundwater flowing into the domain has been altered in the upstream area, for example, by other GWHPs, while scenario 1 represents the case where no GWHPs are present in the upstream area.

4. Results

In this section, the results of the optimization scenarios are presented and analyzed. Table 2 summarizes the results of the optimization scenario 1. For all 15 different initializations, i.e. the first 10 top and 5 random LHS samples (see section 2.2.6), the number of optimization iterations n_{iter} as well as the initial and final values of the functional of interest are provided. In addition to the total number of iterations, the number of iterations for each value of the penalty factor α is also given. For the first two values of α, i.e. $\alpha = 0$ and $\alpha = 0.1$, the number of iterations almost always reaches the predefined maximum number of 50. Thereafter, the number of iterations tends to decrease as the value of α increases, and is usually lowest for the largest α. This means that the main progress in optimization, i.e. the largest changes in the well layout, are achieved during the stages with smallest penalty factor, where violation of the constraints related to restricted areas (see 2.2.3) carries little or no penalty. Considering the functional of interest, its final values are always smaller than the initial values. Since the functional is defined as the negative sum of the groundwater temperatures at all extraction wells, this means that the sum of these temperatures is maximized and increases by a few degrees, e.g. from approx. 89°C to 93°C for the 1st top sample. The only exception to functional improvement is the 6th top sample, where the final value is positive. This means that the solution is not feasible and some of the wells are located within restricted areas, resulting in an increased penalty and therefore shifting the functional into positive range. A further analysis of this special case is carried out later in this section with the help of visualizations. The blue color in Table 2 indicates the two best optimal solutions, which are obtained for the 1st top and the 4th random initialization samples. While these two samples lead to almost identical solutions, it is evident that initialization plays a significant role and that the problem has many local minima. However, using multiple top samples for initialization seems to be a good strategy for reliably reaching or getting close to the global optimum. This is further supported by the fact that the 4th random sample in this case is actually equal to the 13th top sample, which means that this sample would also be one of the top initialization samples if 15 instead of first 10 top samples were used for initialization.

The well layout changes during the optimization iterations for the 1st top sample in optimization scenario 1 are depicted in Figure 10a. Extraction and injection wells are denoted with circles and crosses, and the dark blue and yellow colors represent the first and last iterations, respectively. This notation of wells and

Table 2: Results for optimization scenario 1.

Sample		Nr. of iterations						Functional of interest	
Type	Nr.	$\alpha = 0$	$\alpha = 0.1$	$\alpha = 1$	$\alpha = 10$	$\alpha = 100$	Total	Initial	Final
Top	1	50	47	4	14	1	116	-89.0773	-93.0678
	2	50	50	50	27	8	185	-88.4074	-92.7604
	3	50	50	37	14	12	163	-88.2872	-92.2075
	4	50	50	33	4	5	142	-87.8936	-88.6561
	5	50	50	50	25	6	181	-87.8581	-91.6815
	6	50	50	50	37	6	193	-87.6945	14.8968
	7	50	50	50	50	16	216	-87.6555	-92.3777
	8	50	50	18	50	18	186	-87.5232	-92.8066
	9	50	50	50	50	44	244	-87.4092	-91.9520
	10	50	50	42	7	7	156	-87.4081	-92.1422
Random	1	50	50	44	3	5	152	-84.8632	-90.0143
	2	50	50	50	48	6	204	-85.3343	-90.6592
	3	50	50	50	37	9	196	-85.8546	-92.7686
	4	50	50	25	14	1	140	-87.3253	-93.0817
	5	50	50	33	4	5	142	-82.7233	-88.6561

iterations is used throughout the work. The corresponding groundwater temperature field and well locations for the initial and final (optimal) well layout are presented in Figure 10b. In the optimal solution, wells are placed mainly on the edges of the plots or in their corners. The extraction wells are placed within the regions of high groundwater temperature. To establish such regions, in the optimal well layout all injection wells are grouped within an interior region of the domain. As a result, negative well interactions are minimized and temperatures at the extraction wells are maximized, which is the optimization goal.

To further compare different initialization patterns, changes in well layout during optimization for three samples are shown in Figure 11. The following samples are presented: 4th random, which yields one of the two best optimal solutions in addition to the 1st top sample; 6th top, where the solution is not feasible; and 1st random, with one of the inferior feasible solutions. Comparing the 4th random (see Figure 11a) and 1st top (see Figure 10a) samples, it can be seen that they result in nearly identical optimal well layouts, particularly in the case of extraction wells. For this reason, the final value of the functional of interest is almost the same for the two cases. As mentioned earlier, the 6th top initialization sample produces a positive final functional of interest, i.e. an infeasible solution. The extraction well of system 2, which is marked with a red circle in Figure 11b, is placed within the restricted area, i.e. too close to a building. This causes a large penalty and thus increases the functional of interest. The reason why the extraction well is "captured" in a restricted area is the combination of hard and soft optimization constraints. The hard constraints, such as the minimum distance constraint (21), are those that are imposed directly within the optimization algorithm and, therefore, must be satisfied in each optimization iteration. The soft constraints, such as the constraint over restricted areas (22), are represented with penalty terms and do not have to

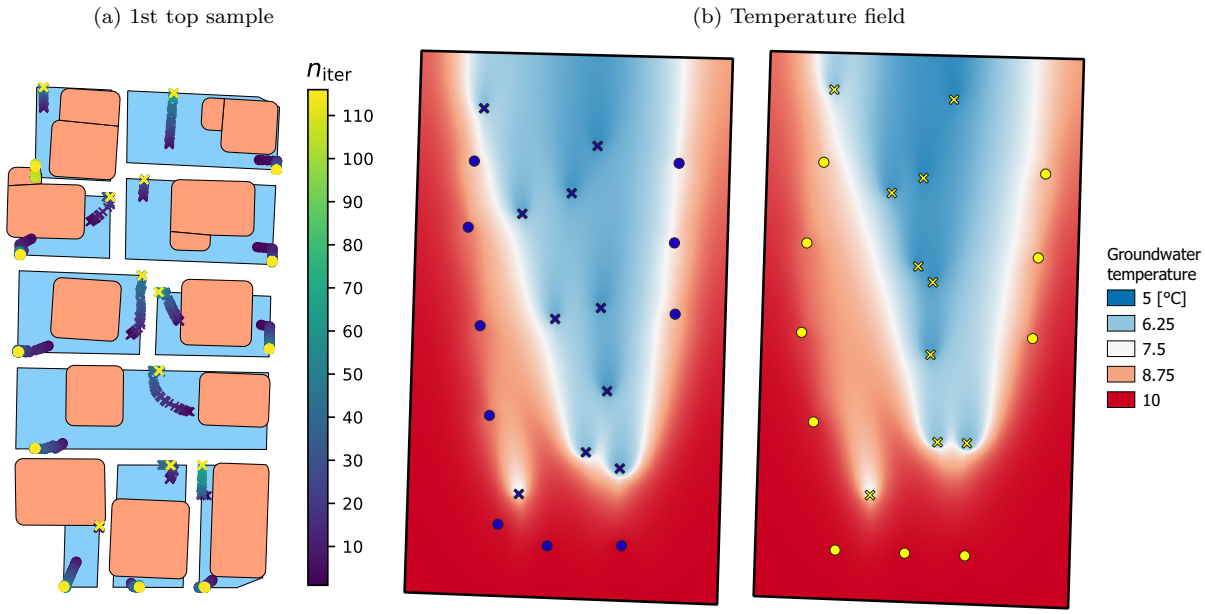


Figure 10: Optimal well layout for optimization scenario 1: (a) Well positions through optimization iterations. Extraction and injection wells are depicted with circles and crosses, respectively. The colors in the legend represent optimization iterations, with dark blue and yellow corresponding to the first and last iteration (solution), respectively. (b) Groundwater temperature field and well locations for the initial (left) and final/optimal (right) well layout.

be satisfied in all optimization iterations. Nevertheless, by increasing the penalty factor, soft constraints should be also met in the final solution. This can be seen in Figure 11b, where the considered extraction well initially "moves" more into the restricted area and after a certain number of iterations tries to leave it. However, the "escape" is not successful, since the distance between the extraction and the corresponding injection well reaches the minimum value, which is represented by a hard constraint and must be always fulfilled. Figure 11c shows the optimal well layout for one of the inferior local optima. Compared to the best optimal solutions, i.e. the 4th random and 1st top, the final well layout differs significantly.

Table 3 summarizes the results of the optimization scenario 2 (see section 3.2). The number of optimization iterations and the initial and final functional of interest are provided for all 15 initialization samples. Similar to optimization scenario 1, the number of iterations almost always reaches the maximum for the two lowest penalty factors, $\alpha = 0$ and $\alpha = 0.1$, and thereafter tends to decrease as α increases. The two best optimal solutions are indicated in blue color and correspond to the 7th and 5th top samples. In addition, the three subsequent best solutions are also obtained from the top samples, namely: 6th, 10th and 1st, respectively. These results reaffirm that using multiple top samples for initialization rather than randomly selecting feasible samples is a valid strategy leading to the global optimum. A feasible solution is found for all 15 samples and the functional of interest has evidently improved. The sum of groundwater temperatures

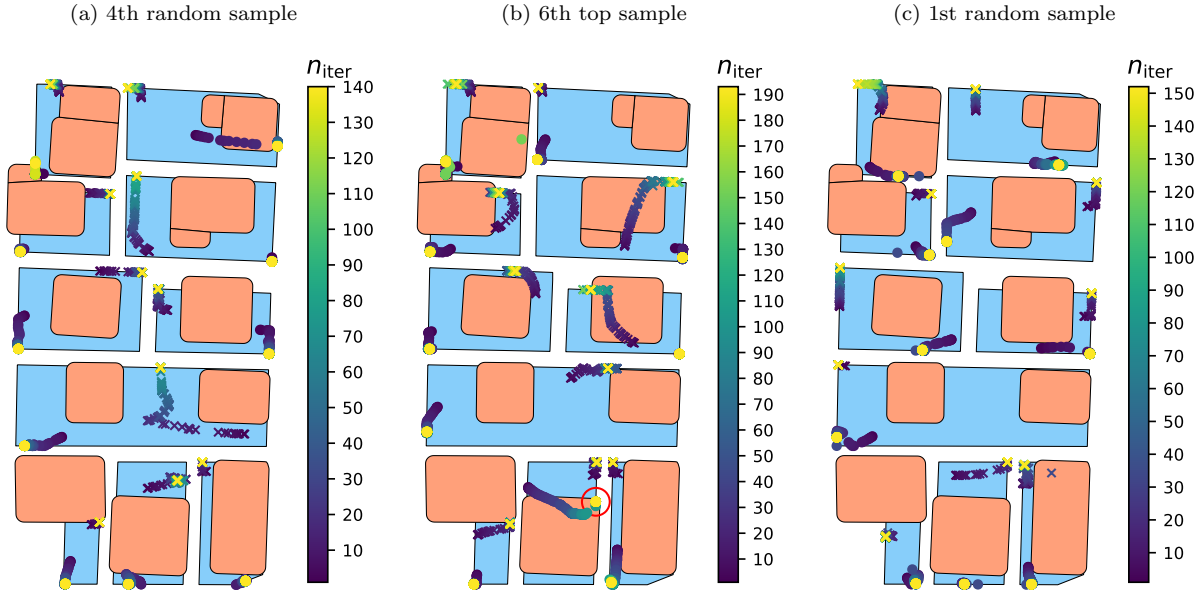


Figure 11: Well positions through optimization iterations for optimization scenario 1. Extraction and injection wells are depicted with circles and crosses, respectively. The colors in the legend represent optimization iterations, with dark blue and yellow corresponding to the first and last iteration (solution), respectively.

at all extraction wells increases by a several degrees, e.g. from approx. 93.3°C to 99.6°C for the 7th top sample. Comparing initial and final functional, the improvement in scenario 2 is larger on average than in scenario 1. This means that the potential for improving well layouts is generally influenced by hydro-geological conditions. However, it should be noted that the final functional values between the two scenarios are not comparable, as the temperature of the groundwater flowing into the area is different.

Changes in well layout during optimization for the 7th top sample, which results in the best optimum in optimization scenario 2, are shown in Figure 12a. The accompanying initial and optimal temperature fields, including well locations, are presented in Figure 12b. Similar to optimization scenario 1, the injection wells are grouped in an interior region of the domain. The only exception is the injection well of the system 1, which does not belong to this cold region. The extraction wells are "moved" to regions with higher groundwater temperatures. The extraction wells on the left side of the domain are not placed in the plot corners as in scenario 1, but follow the patterns in the groundwater temperature field, as shown in Figure 13a. These results demonstrate that: first, hydro-geological conditions, such as the natural groundwater temperature, can significantly influence the optimal well layout; and second, the proposed optimization approach successfully integrates such conditions. Moreover, the temperature fields shown in Figure 10b and 12b indicate that thermal advection plays a significant role in heat transport, which was expected given that the groundwater velocity is relatively high in the study area.

Table 3: Results for optimization scenario 2.

Sample		Nr. of iterations						Functional of interest	
Type	Nr.	$\alpha = 0$	$\alpha = 0.1$	$\alpha = 1$	$\alpha = 10$	$\alpha = 100$	Total	Initial	Final
Top	1	50	50	41	34	3	178	-94.9388	-99.0102
	2	50	50	32	23	1	156	-94.2972	-98.1109
	3	50	50	13	25	1	139	-93.8563	-98.2430
	4	50	50	50	35	8	193	-93.5070	-97.9084
	5	50	50	32	50	50	232	-93.4840	-99.6244
	6	50	50	7	50	22	179	-93.4203	-99.4235
	7	50	50	50	7	47	204	-93.3522	-99.6396
	8	50	50	28	1	1	130	-93.3488	-97.1548
	9	50	50	24	22	1	147	-93.3085	-98.7915
	10	50	50	7	50	11	168	-93.2896	-99.1492
Random	1	50	50	43	38	6	187	-91.8329	-97.9626
	2	50	50	50	50	12	212	-91.4544	-97.4910
	3	50	47	2	40	8	147	-91.7123	-98.8106
	4	50	50	10	50	22	182	-92.2810	-98.9850
	5	50	50	45	7	6	158	-88.8350	-97.4986

Figure 13 also depicts changes in well layout during optimization for the following two samples: 1st top, which has the best initial functional but does not yield the best optimal solution and 3rd random that delivers an inferior feasible solution. The example in Figure 13c also demonstrates that wells, such as the injection well of GWHP 8, can switch sides of the restricted areas during optimization. This is an advantage in the context of global optimization, since the well placement is not limited by the initial relative position to restricted areas.

Figure 14 shows the optimization progress over all iterations. Results obtained with the 1st and 7th top initialization samples are presented for optimization scenarios 1 and 2, respectively. In addition to the evolution of the functional of interest J, changes in groundwater temperatures T at all extraction wells during the optimization are displayed. Iterations with different penalty factors α are indicated with different background colors. Comparing the initial values (iteration 0) with the final values, it is noticeable that the temperatures at extraction wells have increased and at the same time the functional has decreased. This inverse behavior of temperatures and the functional follows from the definition of the functional. According to its definition in (28a), the functional of interest consists of a negative sum of the temperatures at all extraction wells and a penalty term related to restricted areas. The main advance in temperature rise takes place during the $\alpha = 0$ and partially during the $\alpha = 0.1$ stages. Thereafter, the temperatures change only slightly for higher α values. The largest value drop of the functional also occurs at $\alpha = 0$. Additionally, oscillations occur in the functional for some larger α values. The reason for this is that the optimization algorithm uses too large an optimization step and some of wells end up in one of restricted areas, which activates the penalty and increases the functional drastically. However, the algorithm automatically reacts

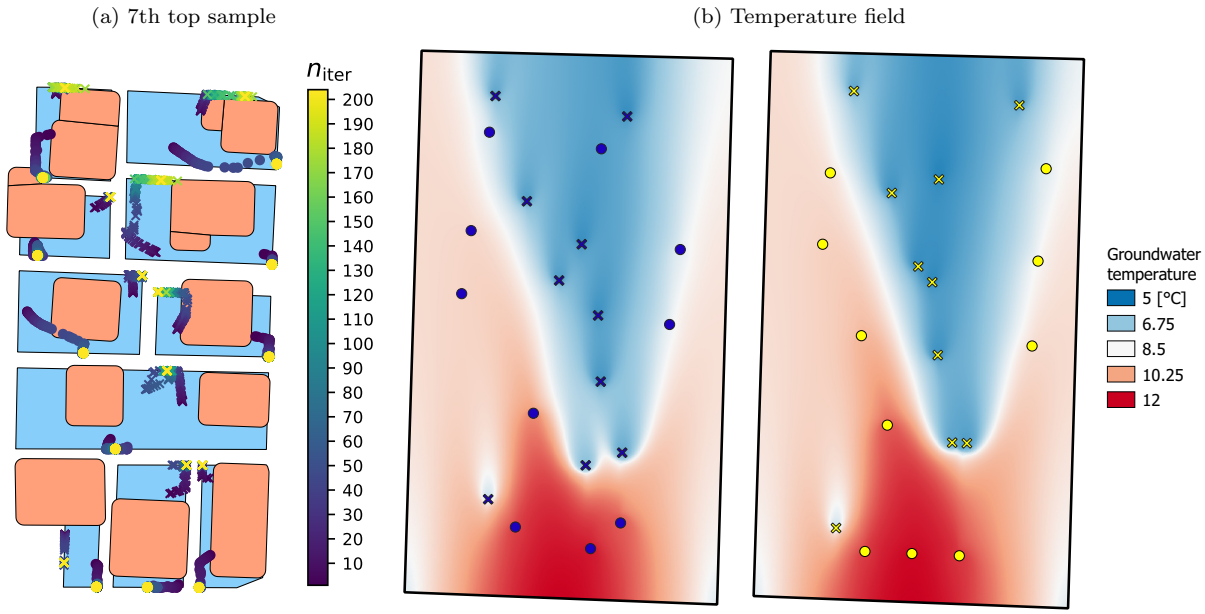


Figure 12: Optimal well layout for optimization scenario 2: (a) Well positions through optimization iterations. Extraction and injection wells are depicted with circles and crosses, respectively. The colors in the legend represent optimization iterations, with dark blue and yellow corresponding to the first and last iteration (solution), respectively. (b) Groundwater temperature field and well locations for the initial (left) and final/optimal (right) well layout.

to this and quickly reduces the functional again. Furthermore, it should be noted that the computational cost increases with increasing α values. As an indicative example, one optimization iteration takes about 2 min and up to 7-9 min for $\alpha = 0$ and $\alpha = 100$, respectively, when running in parallel on 20 cores of Intel Xeon Processor (Skylake, IBRS), 2394 MHz, 88GB of RAM. There is potential for a further reduction in computational time by tuning the parameters of the optimization algorithm, improving the parallelization, or introducing mesh adaptivity techniques to more efficiently focus resolution where needed [45].

Finally, to quantify the well layout improvements after optimization, a benchmark, i.e. non-optimized well layout, is required. It should be noted here that the initial well layouts are generally not the non-optimized benchmark as they are part of the optimization, i.e. the strategy to reach the global optimum. Therefore, for each optimization scenario, the initial sample with the highest functional value of all feasible samples (see section 2.2.6) is used as the non-optimized benchmark. Comparing this benchmark to the final solutions, the functional of interest has changed from approx. $-79.3°C$ to $-93.1°C$ and from $-85.7°C$ to $-99.6°C$ in the scenario 1 and 2, respectively. This means that the sum of groundwater temperatures at all extraction wells has increased by almost $14°C$ in both scenarios after the optimization, which can significantly improve the efficiency of GWHPs.

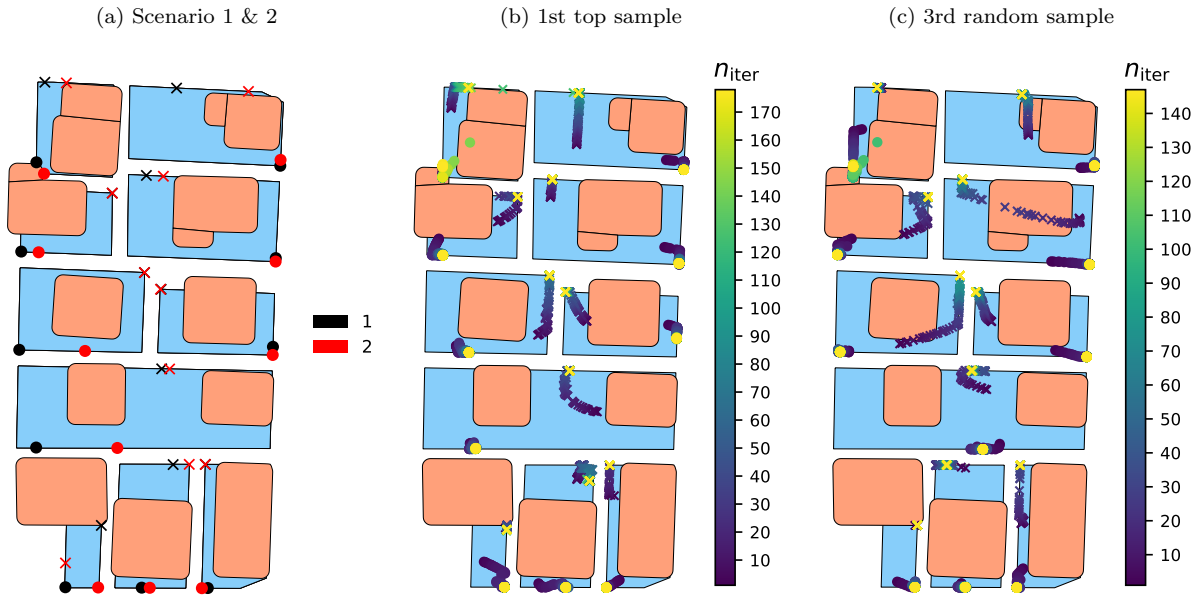


Figure 13: Optimal well layout: (a) Final well positions for optimization scenario 1 (black) and 2 (red) for the samples top 1 and 7, respectively. (b) Well positions through optimization iterations for optimization scenario 2. Extraction and injection wells are depicted with circles and crosses, respectively. The colors in the legend represent optimization iterations, with dark blue and yellow corresponding to the first and last iteration (solution), respectively.

5. Discussion

The results demonstrate that the proposed method can successfully determine the optimal well layout of multiple GWHPs that maximizes groundwater temperatures at all extraction wells. The comparison of the results between optimization scenarios shows that the hydro-geological conditions are an important factor for the optimal well layout and are correctly considered by the method. Furthermore, the proposed multi-start initialization strategy is successful in robustly supporting the attainment of an optimal solution that is closer to the global optima than that obtainable from a random or naively chosen starting configuration. However, the new method has some limitations, which are discussed in the following sections along with future work.

5.1. Critical reflection

The assumptions used to simplify the optimization problem in this work can be divided into two groups: those related to physical phenomena and the conceptual ones. The first are described in section 2.1 and represent reasonable assumptions for the problem under consideration, such as the approximation that the water density remains constant. The conceptual assumptions are the main assumptions that significantly reduce the problem complexity and are therefore discussed in the following.

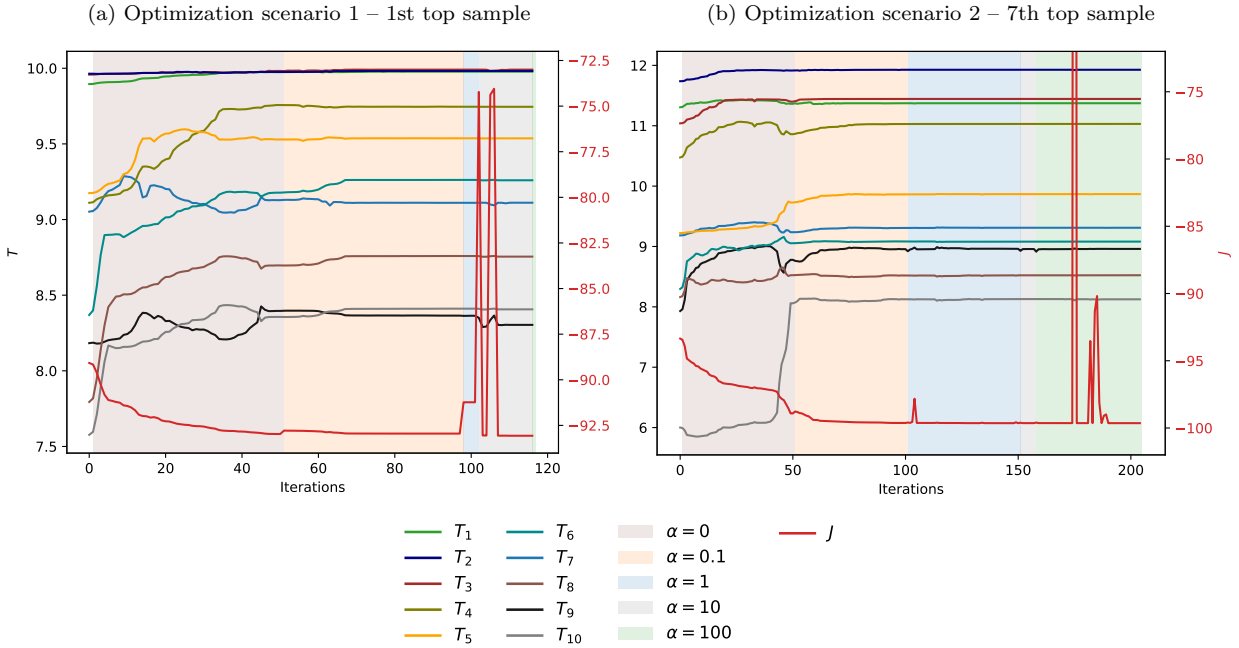


Figure 14: Optimization progress: groundwater temperatures at all extraction wells and the functional of interest J through optimization iterations. Different background colors correspond to different values of the penalty factor α.

In this work only a steady state solution for the groundwater simulation is considered within the optimization procedure. This simplifies the optimization and speeds up the entire process considerably, since only stationary forward and adjoint PDEs are solved in each optimization iteration. In the time-dependent case, both the forward and adjoint PDEs are time-dependent and require appropriate time discretization. Depending on the selected time horizon and time steps, each optimization iteration becomes more time-consuming and memory-intensive compared to the steady state. The time-dependent case, however, is more realistic, as the seasonal changes in GWHP use, e.g. an increased heating demand in winter, as well as the environmental conditions, such as heat fluxes from the surface, can be taken into account [46]. Furthermore, this work assumes a constant, predefined temperature of the re-injected water at injection wells. This should be replaced by a constant temperature difference between extraction and injection wells of each system to improve the representation of GWHPs in the numerical simulation model [47]. If this temperature difference is kept constant, the heating power provided for each GWHP corresponds to that from Table 1.

The approach introduced here uses a vertically averaged 2D representation of the aquifer. To fully take into account all the complexities present in urban aquifers, a 3D numerical model is required [48]. However, the 2D model is, on the one hand, significantly less computationally complex and, on the other hand, should deliver sufficiently good results. It should also be noted that many aquifer parameters, such as the hydraulic conductivity or thermal dispersion factors, are based on indirect measurements and are therefore subject to

uncertainties [49]. It is important to analyze how these parameter uncertainties affect the optimal solution. Such an analysis can be done in two ways, either by including the uncertainties in the optimization, i.e. solving a stochastic PDECO problem, or by performing a parameter-based sensitivity analysis with the optimal solution. This could help to find the minimum data quality required for optimization purposes or to define robust optimal solutions.

5.2. Outlook

One of the first future steps is to include the time dependencies into the optimization, i.e. to consider time-dependent PDECO problem. The solution to this problem can then be compared with the optimal solution from the stationary PDECO to assess how sufficient and robust the stationary case is for optimization purposes. Furthermore, since the groundwater simulation has been simplified by considering a 2D vertically averaged aquifer, a future goal is to use a full 3D model to analyze optimal solutions from the 2D model. For example, one can introduce random vertical heterogeneities in the aquifer to evaluate the robustness of the 2D-based optimal well layout.

Finally, the presented method has several other possible future applications, such as:

- Optimization of large GWHPs with more than one extraction and injection well, which means finding the optimal number and positioning of wells as well as optimal pumping rates. The method can already be used to find optimal well locations of an individual GWHP with any number of wells. However, if the number of wells and their pumping rates are unknown, these can also be defined as optimization variables.

- Optimization of aquifer thermal energy storage (ATES) systems as these systems have the same working principle as GWHPs, with the exception of utilizing the aquifer as energy storage. Similar to GWHPs, optimal well locations and their pumping rates can be found for ATES systems. In addition, the method can be used to find optimal locations of multiple ATES systems in the areas with high density of such systems [50, 51].

- Finding optimal arrangements of neighboring GWHPs that operate in both modes, i.e. heating and cooling. Since these modes change the groundwater temperature in opposite directions, positive interactions between neighboring systems can arise [52]. Thus, it would be useful to optimally place wells so that the positive synergies are maximized. The method can be applied in this case by including the time dependencies and additional heat sources, i.e. cooling wells.

- Improved quantification of the thermal groundwater potential of the area of interest. This means, for example, determining the maximum number of GWPHs that can be installed in a certain area while complying with all regulatory conditions. Such potential assessments could be integrated into energy

589 system optimization models [53], which are used to find optimal energy transition paths towards CO_2
590 reduction targets.

591 6. Conclusions

592 In this work, a new method for determining the optimal well layout of groundwater heat pumps is
593 presented. The method is a gradient-based optimization that relies on an efficient calculation of the required
594 gradients using the adjoint approach. This enables a large number of continuous optimization variables,
595 i.e. well locations, to be considered simultaneously. An integral part of this optimization concept is the
596 numerical simulation of the groundwater flow and heat transport based on finite elements. The new method
597 is implemented using Firedrake and dolfin-adjoint, which are open-source frameworks for numerically solving
598 PDEs using FEM and generating adjoints, respectively. Since the underlying PDE-constrained optimization
599 problem is non-convex and has many local optima, a robust initialization strategy is also proposed. The
600 strategy is to use multiple starting well layouts, which are obtained from Latin Hypercube Sampling and
601 have the best values of the functional of interest.

602 The new method is tested on a case study in Munich, Germany, with real data and 10 GWHPs, each
603 with a single well pair. A total of 10 extraction and 10 injection wells are optimally placed to maximize
604 groundwater temperature at all extraction wells. To analyze the influence of hydro-geological conditions
605 on the optimization results, i.e. the optimal well layout, two optimization scenarios were considered, which
606 differ in the temperature of the inflowing groundwater. The results show that the proposed methodology
607 successfully finds optimal well layouts in both scenarios and that hydro-geological conditions can significantly
608 alter the optimal well layout. In both scenarios, the sum of groundwater temperatures at all extraction wells
609 in the optimal well layout is almost 14°C higher than in the non-optimized benchmark.

610 It should be emphasized that the proposed method is the first well layout optimization method that allows
611 for continuous well locations and is not limited by the number of wells. This is a significant improvement
612 compared to the existing methods, which can only consider predefined (discrete) well locations and a small
613 number of wells. In addition, this is the first method used to optimize the well layout of multiple neighboring
614 GWHPs to maximize thermal groundwater potential. The method can also be applied to find optimal well
615 layouts of individual systems with multiple extraction and injection wells. Moreover, the method can be used
616 in various other applications in the future, such as the optimization of ATES systems or the quantification of
617 the thermal potential of aquifers. Finally, the introduced method can serve as a basis for the future optimal
618 management and planning of the geothermal resource groundwater.

619 7. Conflict of interest

620 The authors declare no conflicts of interest.

Acknowledgement

The work presented in this paper has been supported by the German Federal Ministry for Economic Affairs and Energy (BMWi) within the scope of the research project GEO.KW (01184143/1). The authors also acknowledge the TUM Global Incentive Fund 2021 for supporting the collaboration between the Technical University of Munich and Imperial College London.

References

[1] European Commission, 2050 long-term strategy: Climate action, 2020. URL: https://ec.europa.eu/clima/eu-action/climate-strategies-targets/2050-long-term-strategy_en.

[2] A. Bloess, W.-P. Schill, A. Zerrahn, Power-to-heat for renewable energy integration: A review of technologies, modeling approaches, and flexibility potentials, Applied Energy 212 (2018) 1611–1626. doi:10.1016/j.apenergy.2017.12.073.

[3] A. Rinaldi, M. C. Soini, K. Streicher, M. K. Patel, D. Parra, Decarbonising heat with optimal pv and storage investments: A detailed sector coupling modelling framework with flexible heat pump operation, Applied Energy 282 (2021) 116110. doi:10.1016/j.apenergy.2020.116110.

[4] S. J. Self, B. V. Reddy, M. A. Rosen, Geothermal heat pump systems: Status review and comparison with other heating options, Applied Energy 101 (2013) 341–348. doi:10.1016/j.apenergy.2012.01.048.

[5] V. Somogyi, V. Sebestyén, E. Domokos, A. Zseni, Z. Papp, Thermal impact assessment with hydrodynamics and transport modeling, Energy Conversion and Management 104 (2015) 127–134. doi:10.1016/j.enconman.2015.04.045.

[6] J. Kim, Y. Nam, A numerical study on system performance of groundwater heat pumps, Energies 9 (2016) 4. doi:10.3390/en9010004.

[7] F. Böttcher, K. Zosseder, Thermal influences on groundwater in urban environments – A multivariate statistical analysis of the subsurface heat island effect in Munich, Sci. Total Environ. 810 (2021) 152193. URL: https://doi.org/10.1016/j.scitotenv.2021.152193. doi:10.1016/j.scitotenv.2021.152193.

[8] K. Menberg, P. Bayer, K. Zosseder, S. Rumohr, P. Blum, Subsurface urban heat islands in german cities, The Science of the total environment 442 (2013) 123–133. doi:10.1016/j.scitotenv.2012.10.043.

[9] A. Herbert, S. Arthur, G. Chillingworth, Thermal modelling of large scale exploitation of ground source energy in urban aquifers as a resource management tool, Applied Energy 109 (2013) 94–103. doi:10.1016/j.apenergy.2013.03.005.

[10] G. Attard, P. Bayer, Y. Rossier, P. Blum, L. Eisenlohr, A novel concept for managing thermal interference between geothermal systems in cities, Renewable Energy 145 (2020) 914–924. doi:10.1016/j.renene.2019.06.095.

[11] A. García-Gil, E. Vázquez-Suñe, E. G. Schneider, J. Á. Sánchez-Navarro, J. Mateo-Lázaro, Relaxation factor for geothermal use development – criteria for a more fair and sustainable geothermal use of shallow energy resources, Geothermics 56 (2015) 128–137. doi:10.1016/j.geothermics.2015.04.003.

[12] J. Epting, F. Böttcher, M. H. Mueller, A. García-Gil, K. Zosseder, P. Huggenberger, City-scale solutions for the energy use of shallow urban subsurface resources – bridging the gap between theoretical and technical potentials, Renewable Energy 147 (2020) 751–763. doi:10.1016/j.renene.2019.09.021.

[13] F. Böttcher, A. Casasso, G. Götzl, K. Zosseder, Tap - thermal aquifer potential: A quantitative method to assess the spatial potential for the thermal use of groundwater, Renewable Energy 142 (2019) 85–95. doi:10.1016/j.renene.2019.04.086.

[14] C. G. Clyde, G. V. Madabhushi, Spacing of wells for heat pumps, Journal of Water Resources Planning and Management 109 (1983) 203–212. doi:10.1061/(ASCE)0733-9496(1983)109:3(203).

[15] J. Hecht-Méndez, M. de Paly, M. Beck, P. Bayer, Optimization of energy extraction for vertical closed-loop geothermal

systems considering groundwater flow, Energy Conversion and Management 66 (2013) 1–10. doi:10.1016/j.enconman.2012.09.019.

[16] M. Beck, P. Bayer, M. de Paly, J. Hecht-Méndez, A. Zell, Geometric arrangement and operation mode adjustment in low-enthalpy geothermal borehole fields for heating, Energy 49 (2013) 434–443. doi:10.1016/j.energy.2012.10.060.

[17] Y.-z. Zhou, Z.-f. Zhou, Simulation of Thermal Transport in Aquifer: A GWHP System in Chengdu, China, Journal of Hydrodynamics 21 (2009) 647–657. doi:10.1016/S1001-6058(08)60196-1.

[18] Q. Gao, X.-Z. Zhou, Y. Jiang, X.-L. Chen, Y.-Y. Yan, Numerical simulation of the thermal interaction between pumping and injecting well groups, Applied Thermal Engineering 51 (2013) 10–19. doi:10.1016/j.applthermaleng.2012.09.017.

[19] S. Lo Russo, M. V. Civita, Open-loop groundwater heat pumps development for large buildings: A case study, Geothermics 38 (2009) 335–345. doi:10.1016/j.geothermics.2008.12.009.

[20] D. K. Park, D. Kaown, K.-K. Lee, Development of a simulation-optimization model for sustainable operation of groundwater heat pump system, Renewable Energy 145 (2020) 585–595. doi:10.1016/j.renene.2019.06.039.

[21] D. Park, E. Lee, D. Kaown, S.-S. Lee, K.-K. Lee, Determination of optimal well locations and pumping/injection rates for groundwater heat pump system, Geothermics 92 (2021) 102050. doi:10.1016/j.geothermics.2021.102050.

[22] H.-J. G. Diersch, FEFLOW, Springer Berlin Heidelberg, Berlin, Heidelberg, 2014. doi:10.1007/978-3-642-38739-5.

[23] J. Bundschuh, M. C. Suárez Arriaga, Introduction to the numerical modeling of groundwater and geothermal systems: Fundamentals of mass, energy, and solute transport in poroelastic rocks, volume 2 of *Multiphysics modeling*, CRC Press, Boca Raton, 2010.

[24] M. Hinze, R. Pinnau, M. Ulbrich, S. Ulbrich, Optimization with PDE constraints, volume 23, Springer Science & Business Media, 2008. URL: http://swbplus.bsz-bw.de/bsz288078012cov.htm.

[25] M. B. Giles, N. A. Pierce, An introduction to the adjoint approach to design, Flow, Turbulence and Combustion 65 (2000) 393–415. URL: https://link.springer.com/article/10.1023/a:1011430410075. doi:10.1023/A:1011430410075.

[26] Bayerisches Landesamt für Umwelt, Planung und Erstellung von Erdwärmesonden: LfU, 2012. URL: https://www.lfu.bayern.de/wasser/merkblattsammlung/teil3_grundwasser_und_boden/doc/nr_372.pdf.

[27] E. Milnes, P. Perrochet, Assessing the impact of thermal feedback and recycling in open-loop groundwater heat pump (GWHP) systems: a complementary design tool, Hydrogeology Journal 21 (2013) 505–514. doi:10.1007/s10040-012-0902-y.

[28] Ö. Yeniay, Penalty function methods for constrained optimization with genetic algorithms, Mathematical and Computational Applications 10 (2005) 45–56. URL: https://www.mdpi.com/133758. doi:10.3390/mca10010045.

[29] L. Blank, E. Meneses Rioseco, A. Caiazzo, U. Wilbrandt, Modeling, simulation, and optimization of geothermal energy production from hot sedimentary aquifers, Computational Geosciences 25 (2021) 67–104. doi:10.1007/s10596-020-09989-8.

[30] R. N. King, K. Dykes, P. Graf, P. E. Hamlington, Optimization of wind plant layouts using an adjoint approach, Wind Energy Science 2 (2017) 115–131. doi:10.5194/wes-2-115-2017.

[31] S. W. Funke, P. E. Farrell, M. D. Piggott, Tidal turbine array optimisation using the adjoint approach, Renewable Energy 63 (2014) 658–673. doi:10.1016/j.renene.2013.09.031.

[32] R. Jin, W. Chen, A. Sudjianto, An efficient algorithm for constructing optimal design of computer experiments, Journal of Statistical Planning and Inference 134 (2005) 268–287. doi:10.1016/j.jspi.2004.02.014.

[33] M. A. Bouhlel, J. T. Hwang, N. Bartoli, R. Lafage, J. Morlier, J. R. Martins, A python surrogate modeling framework with derivatives, Advances in Engineering Software 135 (2019) 102662. doi:10.1016/j.advengsoft.2019.03.005.

[34] F. Rathgeber, D. A. Ham, L. Mitchell, M. Lange, F. Luporini, A. T. T. Mcrae, G.-T. Bercea, G. R. Markall, P. H. J. Kelly, Firedrake, ACM Transactions on Mathematical Software 43 (2017) 1–27. doi:10.1145/2998441.

[35] S. Mitusch, S. Funke, J. Dokken, dolfin-adjoint 2018.1: automated adjoints for fenics and firedrake, Journal of Open

Source Software 4 (2019) 1292. doi:10.21105/joss.01292.

[36] M. G. Trefry, C. Muffels, Feflow: A finite-element ground water flow and transport modeling tool, Ground Water 45 (2007) 525–528. doi:10.1111/j.1745-6584.2007.00358.x.

[37] D. Kraft, K. Schnepper, SLSQP—a nonlinear programming method with quadratic programming subproblems, DLR, Oberpfaffenhofen 545 (1989).

[38] P. Virtanen, R. Gommers, T. E. Oliphant, M. Haberland, T. Reddy, D. Cournapeau, E. Burovski, P. Peterson, W. Weckesser, J. Bright, S. J. van der Walt, M. Brett, J. Wilson, K. J. Millman, N. Mayorov, A. R. J. Nelson, E. Jones, R. Kern, E. Larson, C. J. Carey, İ. Polat, Y. Feng, E. W. Moore, J. VanderPlas, D. Laxalde, J. Perktold, R. Cimrman, I. Henriksen, E. A. Quintero, C. R. Harris, A. M. Archibald, A. H. Ribeiro, F. Pedregosa, P. van Mulbregt, Scipy 1.0: fundamental algorithms for scientific computing in python, Nature Methods 17 (2020) 261–272. URL: https://www.nature.com/articles/s41592-019-0686-2?report=reader. doi:10.1038/s41592-019-0686-2.

[39] K. Zosseder, M. Kerl, A. Albarrán-Ordás, M. Gossler, A. Kiecak, L. Chavez-Kus, Die hydraulischen Grundwasserverhältnisse des quartären und des oberflächennahen tertiären Grundwasserleiters im Großraum München, Geol. Bavarica 122 (2022) 199. URL: https://www.bestellen.bayern.de/shoplink/91122.htm.

[40] A. Albarrán-Ordás, K. Zosseder, The Di models method: geological 3-D modeling of detrital systems consisting of varying grain fractions to predict the relative lithological variability for a multipurpose usability, Bull. Eng. Geol. Environ. 81 (2022). doi:10.1007/s10064-021-02538-2.

[41] A. Albarrán-Ordás, K. Zosseder, Geostatistische reliefmodellierung der quartären grundwasserleiterbasis in der münchener schotterebene unter verwendung von massendaten, Zeitschrift der Deutschen Gesellschaft für Geowissenschaften 171 (2020) 1–19. URL: http://dx.doi.org/10.1127/zdgg/2020/0206. doi:10.1127/zdgg/2020/0206.

[42] M. Theel, P. Huggenberger, K. Zosseder, Assessment of the heterogeneity of hydraulic properties in gravelly outwash plains: a regionally scaled sedimentological analysis in the Munich gravel plain, Germany, Hydrogeol. J. 28 (2020) 2657–2674. doi:10.1007/s10040-020-02205-y.

[43] A. Molar-Cruz, UrbanHeatPro, https://github.com/tum-ens/UrbanHeatPro, 2020.

[44] C. Geuzaine, J.-F. Remacle, Gmsh: A 3-d finite element mesh generator with built-in pre- and post-processing facilities, International Journal for Numerical Methods in Engineering 79 (2009) 1309–1331. doi:10.1002/nme.2579.

[45] J. Wallwork, A. Angeloudis, N. Barral, L. Mackie, S. Kramer, M. Piggott, Tidal Turbine Array Modelling using Goal-Oriented Mesh Adaptation, California Digital Library (CDL), 2022. doi:10.31223/x5h06b.

[46] F. Stauffer, P. Bayer, P. Blum, N. M. Giraldo, W. Kinzelbach, Thermal use of shallow groundwater, CRC Press, Boca Raton, Fla., 2014.

[47] S. Muela Maya, A. García-Gil, E. Garrido Schneider, M. Mejías Moreno, J. Epting, E. Vázquez-Suñé, M. Á. Marazuela, J. Á. Sánchez-Navarro, An upscaling procedure for the optimal implementation of open-loop geothermal energy systems into hydrogeological models, Journal of Hydrology 563 (2018) 155–166. doi:10.1016/j.jhydrol.2018.05.057.

[48] J. Epting, P. Huggenberger, Unraveling the heat island effect observed in urban groundwater bodies - Definition of a potential natural state, J. Hydrol. 501 (2013) 193–204. doi:10.1016/j.jhydrol.2013.08.002.

[49] L. W. Gelhar, C. Welty, K. R. Rehfeldt, A Critical Review of Data on Field-Scale Dispersion in Aquifers, Water Resour. Res. 28 (1992) 1955–1974. doi:10.1029/92WR00607. arXiv:arXiv:1011.1669v3.

[50] M. Bloemendal, T. Olsthoorn, F. Boons, How to achieve optimal and sustainable use of the subsurface for aquifer thermal energy storage, Energy Policy 66 (2014) 104–114. doi:10.1016/j.enpol.2013.11.034.

[51] M. Bloemendal, M. Jaxa-Rozen, T. Olsthoorn, Methods for planning of ates systems, Applied Energy 216 (2018) 534–557. doi:10.1016/j.apenergy.2018.02.068.

[52] A. García-Gil, M. Mejías Moreno, E. Garrido Schneider, M. Á. Marazuela, C. Abesser, J. Mateo Lázaro, J. Á. Sánchez Navarro, Nested shallow geothermal systems, Sustainability 12 (2020) 5152. doi:10.3390/su12125152.

[53] S. Halilovic, L. Odersky, T. Hamacher, Integration of groundwater heat pumps into energy system optimization models, Energy 238 (2022) 121607. doi:10.1016/j.energy.2021.121607.

[54] Kelsey Jordahl, Joris Van den Bossche, Martin Fleischmann, Jacob Wasserman, James McBride, Jeffrey Gerard, Jeff Tratner, Matthew Perry, Adrian Garcia Badaracco, Carson Farmer, Geir Arne Hjelle, Alan D. Snow, Micah Cochran, Sean Gillies, Lucas Culbertson, Matt Bartos, Nick Eubank, maxalbert, Aleksey Bilogur, Sergio Rey, Christopher Ren, Dani Arribas-Bel, Leah Wasser, Levi John Wolf, Martin Journois, Joshua Wilson, Adam Greenhall, Chris Holdgraf, Filipe, François Leblanc, geopandas/geopandas: v0.8.1, 2020. doi:10.5281/ZENODO.3946761.

[55] M. Hintermüller, M. Hinze, Moreau–Yosida Regularization in State Constrained Elliptic Control Problems: Error Estimates and Parameter Adjustment, SIAM Journal on Numerical Analysis 47 (2009) 1666–1683. doi:10.1137/080718735.

Appendix A. Coefficients for linear control constraints

Linear control constraints (18) are generated automatically in the code using the following steps:

1. The geometry of plots is read from shape files using the Python library GeoPandas [54]. The result is a list of vertices for each convex plot.
2. The vertices are then used to define linear functions that correspond to the edges of plots.
3. Inequality constraints are defined based on geometric relations and the linear functions obtained previously.

In the second step, the linear function corresponding to the edge e_{ij} between two vertices v_i and v_j is obtained from the equation of a line through two points:

$$y = k_{ij} \cdot x + n_{ij} \tag{A.1a}$$

$$k_{ij} = \frac{y_j - y_i}{x_j - x_i} \tag{A.1b}$$

$$n_{ij} = \frac{y_i \cdot x_j - y_j \cdot x_i}{x_j - x_i} \tag{A.1c}$$

where $v_i = (x_i, y_i)$ and $v_j = (x_j, y_j)$. It should be noted that in the case of $x_i = x_j = x_\perp$ the previous formulas for k_{ij} and n_{ij} are not applicable since the function becomes $y = x_\perp$.

In the third step, the inequality constraint for each edge is obtained from the function (A.1a) by replacing the equality sign with $\leq$ or $\geq$. The inequality sign is selected based on a relative geometric positions of the corresponding edge e_{ij} and an arbitrary point $p_c = (x_c, y_c)$ within the convex plot (polygon). An example plot with an internal point p_c and an edge e_{ij} is depicted in Figure A.15a. If the edge e_{ij} lies "below" the point p_c then $=$ in (A.1a) is replaced by $\geq$ and, otherwise it is replaced by $\leq$ if the edge is "above" the point. The "below" and "above" means respectively negative and positive y-axis sections $m_c = y(x_c)$ of the function corresponding to that edge on an auxiliary coordinate system, whose origin is the point p_c (Figure A.15b). The special case $y = x_\perp$ must be separately considered, since there is no intersection with

y-axis here (Figure A.15c). In this case, if $x_c \leq x_\perp$ the inequality constraint reads as $x \leq x_\perp$ and, otherwise, the constraints becomes $x \geq x_\perp$. It should be noted that the point p_c can be chosen arbitrarily as far as it is inside the plot, but here the geometrical centroids of plots are used since they are easy to obtain from shape files.

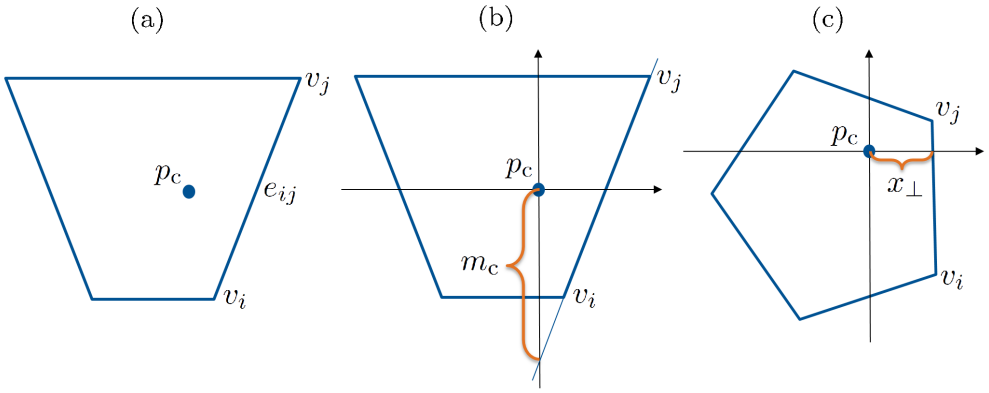


Figure A.15: Geometric relations between an edge e_{ij} and a point p_c within the plot.

Appendix B. State constraints

Once the order of installation of GWHPs is established, a new set of constraints should be added to reflect the regulations on negative interference between neighboring GWHP systems. As already mentioned, neighboring GWHPs can influence each other in such a way that upstream GWHPs change the groundwater temperature at extraction wells of downstream GWHPs. In some countries, the approval ordinance stipulates that the temperature change (due to the new upstream systems) at the extraction well of an existing GWHP must be less than a specified constant threshold value $\mathrm{T_{diff}}$. In this work, the area of interest is located in Bavaria, Germany, where $\mathrm{T_{diff}} = 1$ [K] [26]. The corresponding constraints are given as follows:

$$T_{\mathrm{n}}(\mathbf{x}_i^{\mathrm{ext}}) - T(\mathbf{x}_i^{\mathrm{ext}}) \leq \mathrm{T_{diff}} \quad \forall i \in \{1, ..., N_{\mathrm{exis}}\} \tag{B.1}$$

where $T_{\mathrm{n}}(\mathbf{x}_i^{\mathrm{ext}})$ is the natural groundwater temperature at the extraction well of GWHP i; $T(\mathbf{x}_i^{\mathrm{ext}})$ the temperature after new systems have been installed upstream; N_{exis} the number of existing GWHPs. The temperature field T_{n} can be obtained by solving the underlying PDE system without any new GWHPs and, thus, represents a constant parameter in the optimization problem. It is important to note that the current system for installing (licensing) new GWHPs works on a first-come-first-served basis. Therefore, the regulation described above is only applied to new systems to check whether they have a negative impact on already existing downstream GWHPs.

In (B.1) the temperature fields (functions) are evaluated at the positions of extraction wells, which means that the Dirac delta function is applied in the same way as in (16). However, it should be noted that $\mathbf{x}_i^{\mathrm{ext}}$

in (B.1) are no longer control variables, but only constant values, since the existing GWHPs are "fixed" and not part of the optimization. Moreover, the constraints (B.1) include the state T and, thus, cannot be explicitly defined in the reduced formulation (11). There are several approaches to dealing with state constraints in PDECO problems, including the penalty-based approach.

The state constraints (B.1) can be replaced by adding a penalty term P_T to the original functional of interest (16). In the first step, the constraints are reformulated as follows:

$$\int_\Omega s_1(\mathbf{x}_i^{\text{ext}})\,\mathrm{d}\Omega \leq \int_\Omega s_2(T, \mathbf{x}_i^{\text{ext}})\,\mathrm{d}\Omega \tag{B.2}$$

where $s_1(\mathbf{x}_i^{\text{ext}}) = (T_{\text{n}}(\mathbf{x}) - \mathrm{T}_{\text{diff}}) \cdot \delta(\mathbf{x} - \mathbf{x}_i^{\text{ext}})$ and $s_2(T, \mathbf{x}_i^{\text{ext}}) = T(\mathbf{x}) \cdot \delta(\mathbf{x} - \mathbf{x}_i^{\text{ext}})$. Thereafter, the penalty term is defined as:

$$P_T = \gamma \cdot \sum_{i=1}^{N} \int_\Omega (\max\{0, s_1^i - s_2^i\})^2\,\mathrm{d}\Omega \tag{B.3}$$

where $s_1^i = s_1(\mathbf{x}_i^{\text{ext}})$, $s_2^i = s_2(T, \mathbf{x}_i^{\text{ext}})$, and γ is a penalty scaling factor. This type of penalty is similar to the Moreau-Yosida type of regularization terms used in state-constrained optimization problems [55]. The penalty term P_T becomes zero when the constraints (B.1) are met, and otherwise scales quadratically with the constraints violation. The maximum function in (B.3) is squared to obtain a smooth function, which is advantageous for gradient-based optimization.